HHS Public Access

Author manuscript

Neurobiol Dis. Author manuscript; available in PMC 2016 May 01.

Published in final edited form as:

Neurobiol Dis. 2015 May ; 77: 173–190. doi:10.1016/j.nbd.2015.02.022.

Increased Cortical Synaptic Activation of TrkB and Downstream Signaling Markers in a Mouse Model of Down Syndrome

RL Nosheny[1,2], **PV Belichenko**[1], **BL Busse**[2], **AM Weissmiller**[1], **V Dang**[3], **D Das**[3], **A Fahimi**[3], **A Salehi**[3], **SJ Smith**[2], and **WC Mobley**[1]

[1]Department of Neurosciences, University of California, San Diego, 9500 Gilman Drive, La Jolla, CA 92093

[2]Department of Molecular and Cellular Physiology, Stanford University, 279 Campus Drive, Stanford, CA 94305

[3]Department of Psychiatry & Behavioral Sciences, Stanford Medical School, VA Palo Alto Health Care System, 3801 Miranda Avenue, Palo Alto, CA 94304

Abstract

Down Syndrome (DS), trisomy 21, is characterized by synaptic abnormalities and cognitive deficits throughout the lifespan and with development of Alzheimer's disease (AD) neuropathology and progressive cognitive decline in adults. Synaptic abnormalities are also present in the Ts65Dn mouse model of DS, but which synapses are affected and the mechanisms underlying synaptic dysfunction are unknown. Here we show marked increases in the levels and activation status of TrkB and associated signaling proteins in cortical synapses in Ts65Dn mice. Proteomic analysis at the single synapse level of resolution using array tomography (AT) uncovered increased colocalization of activated TrkB with signaling endosome related proteins, and demonstrated increased TrkB signaling. The extent of increases in TrkB signaling differed in each of the cortical layers examined and with respect to the type of synapse, with the most marked increases seen in inhibitory synapses. These findings are evidence of markedly abnormal TrkB-mediated signaling in synapses. They raise the possibility that dysregulated TrkB signaling contributes to synaptic dysfunction and cognitive deficits in DS.

Keywords

Down Syndrome; Ts65Dn mice; synapses; BDNF; TrkB; signaling endosomes; cerebral cortex

Corresponding Author: Rachel L. Nosheny, Department of Neurosciences, University of California, San Diego, 9500 Gilman Drive, La Jolla, CA 92093, rnosheny@gmail.com, Tel: 650-468-0619, Fax: 415-668-2864.
Present address of corresponding author: Center for Imaging of Neurodegenerative Diseases, 4150 Clement Street, San Francisco, CA 94121

Introduction

DS, caused by trisomy for chromosome 21, is characterized by delayed physical, cognitive, and motor skill acquisition. Remarkably, the neuropathology of AD occurs essentially universally by the forth decade of life in individuals with DS (Burger and Vogel, 1973; Ellis et al., 1974; Price et al., 1982), and cognitive decline is often evident by the sixth decade (Chapman and Hesketh, 2000; Lai and Williams, 1989). Studies of DS brains consistently demonstrate changes in synapses (Ferrer and Gullotta, 1990; Weitzdoerfer et al., 2001), suggesting the possibility that synaptic dysfunction underlies the cognitive problems associated with DS.

Synaptic dysfunction is also present in the Ts65Dn mouse model of DS (Reeves et al., 1995), which recapitulates both cognitive and neuropathological DS phenotypes. Ts65Dn mice, which are partially trisomic for mouse chromosome 16 in a region orthologous to human chromosome 21, exhibit learning and memory deficits and changes in cortical and hippocampal circuits (Reeves et al., 1995). Synaptic abnormalities include reduced dendritic spine density, increased spine size, increased active zone length in specific synapse subtypes, and decreased levels of pre- and postsynaptic markers. (Belichenko et al., 2004; Chakrabarti et al., 2007; Kurt et al., 2004; Salehi et al., 2006). Increased $GABA_A$ and $GABA_B$-mediated inhibitory neurotransmission is responsible for deficient long term potentiation in hippocampus (Belichenko et al., 2004; Fernandez et al., 2007; Kleschevnikov et al., 2012b; Kleschevnikov et al., 2004; Siarey et al., 1997).

DS and AD brains exhibit increased size and number of Rab5-immunopositive early endosomes; in DS this phenotype is evident during the first year of life (Cataldo et al., 1997; Cataldo et al., 2008; Cataldo et al., 2000; Ginsberg et al., 2010). Enlarged endosomes are also present in neurons in Ts65Dn mice (Cataldo et al., 2003; Salehi et al., 2006). The significance of endosomal abnormalities is undefined. However, trafficking of neurotrophic factors (NTFs), whose signals are conveyed by early endosomes from synaptic terminals to neuronal soma, is disrupted in AD and DS model mice (Cooper et al., 2001b; Salehi et al., 2006). This raises the possibility that changes in endosomes disrupt trafficking of NTF signals. Accordingly, we investigated NTF signaling in Ts65Dn mice.

NTF signaling is important for synaptic development, maintenance, and plasticity, and BDNF-TrkB signaling is especially important for GABAergic neurotransmission (Chen et al., 2011a; Rico et al., 2002; Sanchez-Huertas and Rico, 2011; Seil and Drake-Baumann, 2000; Yamada et al., 2002). We entertained the possibility that this aspect of BDNF-TrkB function may be involved in synaptic structure abnormalities seen in Ts65Dn mice. Herein we identity increases in TrkB signaling in the cerebral cortex of Ts65Dn mice, decipher the sub-cellular location of these abnormalities, and identify affected synapse subtypes. We report that increases in TrkB signaling are present in abnormal endosomes in synapses in Ts65Dn mice. The signaling increases detected predict a role for dysregulation of TrkB signaling in increased inhibitory neurotransmission in this model, and raise the possibility that dysregulation of TrkB signaling also contributes to synaptic dysfunction in DS and AD.

Materials and methods

Animals

Male control (2N) and Ts65Dn littermates mice, carried on a balanced B6 and C3H background, were used for all studies other than AT. Three-month old mice were used for synaptosome studies, and 12 month old mice were used for RT-PCR, BDNF ELISA, and whole cortex western blot studies. Ts65Dn (Ts(1716)65Dn, Jackson Laboratory, Stock #001924) mice have three copies of a fragment of the MMU16 extending from Mrpl39 to Znf295 including App gene. The Ts65Dn mouse colony was maintained by crossing B6EiC3Sn-Ts(1716)65Dn females (Jackson Laboratory) with B6EiC3SnF1/J A/a males (Jackson Laboratory). For AT studies, 12 month old male Ts65Dn × GFP-M and 2N × GFP-M mice were used. To generate 2N and Ts65Dn mice that express green fluorescent protein (GFP), Ts65Dn female mice were crossed to male mice that carry GFP-M transgene (Feng et al., 2000) on a mixed genetic background (C57BL/6J and B6EiC3). Male offspring of this cross were used in the present study. All experiments were conduced in accordance with the National Institutes of Health guidelines for the care and use of animals and an approved animal protocol for the Stanford University Institutional Animal Care and Use Committee and the University of California, San Diego, Institutional Animal Care and Use Committee. All efforts were made to minimize animal stress and discomfort.

Synaptosome preparation

Cortices (n=12 mice per genotype, experiments repeated 2 or 3 times) were collected, pooled (2–3 cortices per sample), and homogenized in homogenization buffer (HB; 0.32 M ultra pure sucrose, 10 mM Tris, 1X Sigma phosphatase inhibitor cocktail 2 and 3, 1X Roche Complete protease inhibitor tablet, pH 7.0). The homogenate was brought up in HB and centrifuged (800xg, 15min, 4°C). The supernatant was run on 2 successive sucrose gradients (0.8M, 1.2M) for 20 minutes using a Beckman L2–65B preparative ultracentrifuge (SW41Ti rotor, 39,000 rpm), to isolate the enriched synaptosomal fraction (ESF). More details are given in (Cataldo et al., 2003; Cooper et al., 2001b; Salehi et al., 2006). See Fig 1 for a schematic describing the flow of experimental procedures.

BDNF treatment of synaptosomes

ESFs were resuspended in ice cold PBS with Ca^{2+} and Mg^{2+}. centrifuged at 12,000g for 1 minute, resuspended in binding buffer, composed of 1mg/ml glucose, 11 mg/ml BSA in Phosphate Buffered Solution (PBS), and incubated with gentle shaking at 37°C for 30 minutes to re-equilibrate ion pumps. BDNF (50ng/ml) or vehicle control (binding buffer alone) was added to ESFs and incubated at 37°C for 30 minutes to allow internalization. Then the ESFs were put on ice and an equal volume of ice cold PBS was added. ESFs were then processed for Western Blot analysis, described below.

BDNF surface-binding assay

In 2 separate experiments, ESFs were isolated (n= 6 preps per condition per experiment, each prep contains 3–5 cortices pooled together), resuspended in ice cold PBS with Ca^{2+} and Mg^{2+}, centrifuged at 12,000g for 1 minute, resuspended in binding buffer (1mg/ml

glucose, 11 mg/ml BSA in DPBS), and incubated with gentle shaking at 37°C for 30 minutes. BDNF was linked to streptavidin Quantum dot 655 conjugate (QD655; Invitrogen, Cat # Q10121MP, Lot 906913) by incubating 5μl BDNF, μl QD655, and 14 μl binding buffer on ice for 30 min, followed by the addition of 4ml binding buffer, to create a 1nM stock solution. QD655 linked to BDNF (QD-BDNF) or QD655 alone (QD-veh) at 50ng/ml was added to ESFs and incubated at 37°C for <5 minutes, then samples were immediately put on ice and washed 3 times in excess cold PBS. ESFs were fixed in 1.6% PFA for 20 min. and washed 3 times in PBS. An equal amount of protein was added to each coverslip. For quantification, the number of QD-positive puncta was counted and normalized to the total number of actin-positive synaptosomes.

Western blot (WB)

ESFs were resuspended in lysis buffer (1% Trion X, 1% NP40, 0.1% SDS, 0.5% Sodium deoxycholate, 1X Roche Complete protease inhibitor cocktail, 1x Sigma phosphatase inhibitor cocktail 2 and 3, 2mM PMSF in DPBS pH 7.4), and lysed for 30 minutes at 4°C with gentle rocking. Lysates were centrifuged at 4°C, 14,000 rpm, 10 minutes and the supernatant was collected as the ESF lysate. 10–80 μg of ESF lysates were loaded onto 4–12% Bis-Tris gels, separated by electrophoresis, and transferred to PVDF membranes. Membranes were blocked with TBST with 5.5% nonfat milk and incubated with primary antibodies in TBST 5.5% nonfat milk overnight, washed in TBS and incubated with HRP-conjugated secondary antibodies in TBST for 1 hour. Immunoreactivity was detected using chemiluminescence, and band density was measured on scanned films using FIJI software (NIH).

Confocal microscopy

30 μl ESF aliquots were dropped onto adhesive coated glass slides and dried overnight at room temperature, creating a spot 7 mm in diameter. Spots were coverslipped using 90% glycerol in water and single-channel confocal microscopy was used for imaging distribution of QD655 in synaptosomes. Slices were examined and scanned in a Radiance 2000 confocal microscope (BioRad, Hertfordshire, UK) attached to a Nikon Eclipse E800 fluorescence microscope. The laser was an argon/krypton mixed gas laser with exciting wavelengths for QD655 (488λ). The emission was registered with 660LP “far-red” filter for QD655. LaserSharp software (BioRad) was used to establish optimal conditions for collecting images. Slices with QD655 were illuminated with UV light for 5 minutes and then studied under the following optimal conditions: the lens was a ×20 objective (Nikon; Plan Apo ×20/0.75); laser power was 100%, 4 optical sections were scanned at 5 μm increments; the zoom factor was 1; scan speed was 500 lps; each optical section was the result of three scans followed by Kalman filtering; the size of the image was 512×512 pixels (i.e. 520×520 μm). Each image was saved as a stack of individual optical sections and as a z-projection. Three images of synaptosomes per ESF sample (with an n=3, this results in a total 9 images per experiment) were analyzed. LaserPix software analysis of the z-projection image of synaptosomes was used to measure the density of QD655 in 520×520 μm area. Digital images were imported, enhanced for brightness and contrast, assembled and labeled in Adobe Photoshop CS2 9.0.2, and archived.

Somatosensory cortex dissection for RT-PCR and ELISA

Mice (12 months old, n=6 for each genotype) were deeply anesthetized with 200 mg/kg pentobarbital and perfused with cold saline. Each brain sample was dissected out, flash-frozen in liquid nitrogen, and stored at −80 C until further processing. In order to isolate frontal cortex (FC), each brain was mounted in OCT (Sakura, Co) and sectioned at −30 C using the cryostat microtome (Leica CM 1950). The somatosensory cortical (S1) region was collected using a 1.6 mm area glass tube. 3–4 punches were collected

RT-PCR

Total RNA was isolated using Trizol (Invitrogen, Carslbad, CA), and treated with DNAse I (Invitrogen) for 10 minutes at 37°C, and heat inactivated at 85°C for 5 minutes. First-strand cDNA synthesis was performed with TaqMan MicroRNA Reverse Transcription Kit (AB, Foster City) and oligo dT (17) s (Invitrogen) in a reaction volume of 20 μl at 42°C for 1 hour, followed by heat inactivation at 85°C for 5 minutes. Real-time polymerase chain reaction was performed by using 1μl of cDNA, 1 μl of 10 μM of primer, and Brilliant III Ultra-Fast SYBR (R) Green QRT-PCR Master Mix (Agilent, CA) to a final volume of 26 μL. The reactions were run as follows: 2 minutes at 95°C initial stage, 45 cycles at 95°C for 15 seconds and 60°C for 30 seconds, followed by the dissociation step (95°C for 1 minute, 55°C for 30 seconds, 95°C for 30 seconds) using the Stratagene MX3005P (Agilent, CA). Melting curve analysis confirmed the specificity in each reaction. The cycle threshold (CT) for TrkB, BDNF, and their normalizers (β-actin, Gapdh, and PPIA) were automatically calculated. The resulting CTs for BDNF and TrkB were normalized to the geometrical average of CTs for β-actin and Gapdh. Student's t test was used to compare the groups and a p value <0.05 was considered significant. Primers (IDT, San Diego, CA) used were as follows:

β-actin: AAATCGTGCGTGACATCAAA (Forward); AAGGAAGGCTGGAAAAGAGC (Reverse)

Gapdh: TGCACCAACTGCTTAGC (Forward); GGCATGGACTGTGGTCATGAG (Reverse)

Bdnf: CATGAAGGCGGCGCCCATGA (Forward); CTGCCCTGGGCCCATTCACG (Reverse)

TrkB: CGCCCTGTGAGCTGAACTCTG (Forward); CTGCTTCTCAGCTGCCTGACC (Reverse)

PPIA: TAT CTG CAC TGC CAA GAC TGA (Forward); CTT CTT GCT GGT CTT GCC ATT (Reverse)

BDNF ELISA

Somatosensory cortices isolated as described above were incubated in lysis buffer (1% Trion X, 1% NP40, 0.1% SDS, 0.5% Sodium deoxycholate, 1X Roche Complete protease inhibitor cocktail, 1x Sigma phosphatase inhibitor cocktail 2 and 3, 2mM PMSF in DPBS pH 7.4), and lysed for 30 minutes at 4°C with gentle rocking. BDNF protein levels were

quantified using ELISA kits (Bosterbio) and values were normalized to total protein levels using a Micro BCA Protein Assay Kit (Thermo).

Dissection of somatosensory cortex for Array Tomography

Dissection, dehydration, and embedding were performed similarly to previously described (Micheva et al., 2010a; Micheva and Smith, 2007). Twelve month old 2N and Ts65Dn mice (n=3 per genotype) were anesthetized with Sodium Pentobarbital and intracardially perfused with DPBS followed by 4% PFA for 1 min. Mice were decapitated and the brains were removed from the skull. The brain was cut in half using a sagittal cut along the midline, and then a 1 mm coronal section was made encompassing the somatosensory cortex.

Dehydration and embedding of tissue for array tomography

The dissected piece of cortex was fixed by immersion in 4% paraformaldehyde and 2.5% sucrose in phosphate-buffered saline (PBS) using rapid microwave irradiation (PELCO 3451 laboratory microwave system; Ted Pella; one cycle of 1 min on–1 min off −1 min on at 100 W and two cycles of 20 sec on–20 sec off–20 sec on at 350 W) and ColdSpot (Ted Pella) set at 15°C. The tissue was then left in the fixative for 30 minutes at room temperature. After rinsing in PBS containing 3.5% sucrose, the tissue was quenched in 50 mM glycine in PBS and then dehydrated in a graded series of ethanol (45 sec each at 350 W in microwave). To preserve GFP fluorescence, the tissue was dehydrated only up to 95% ethanol. The tissue was then infiltrated in hydrophilic acrylic resin (LRWhite) three times, 45 sec each, at 350 W and overnight at 4°C), embedded in gelatin capsules and polymerized at 50°C.

Preparation of cortical arrays

Ribbons of serial ultrathin (100 nm) sections were cut with an ultramicrotome (EM UC6, Leica Microsystems, Wetzlar, Germany) as described (Micheva et al., 2010c). The ribbons were mounted on subbed coverslips (coated with 0.5% gelatin and 0.05% chromium potassium sulfate) and placed on a hot plate at 60°C for 30 minutes.

Fluorescence microscopy and image processing

Sections were imaged on a Zeiss Axio Imager.Z1 Upright Fluorescence Microscope with motorized stage and Axiocam HR Digital Camera as described (Micheva et al., 2010b). Briefly, the region of interest was identified on each section using a 20x objective with custom-made software and imaged at a higher magnification with a Zeiss 63×/1.4 NA Plan Apochromat objective, using the image-based automatic focus capability of the software. The resulting stack of images was exported to ImageJ, aligned and registered using the MultiStackReg plugin and imported back into the Axiovision software to generate a volume rendering as previously described (Micheva et al., 2010a). Briefly, the MultiStackReg plugin of ImageJ was used to register the stacks generated from multiple imaging session with the first session stacks based on the DAPI channel, then a second “within-stack” alignment was applied to all the stacks. Finally, to remove non-linear physical warping introduced into the ribbons by the sectioning process, we used a second ImageJ plugin, Register Virtual Stack Slices, which adapts an algorithm for elastic image registration using vector-spline regularization (Micheva et al., 2010a). For all manuscript figures, images representing

volume renderings were upscaled using bicubic interpolation and adjusted for brightness and contrast. All image adjustments were performed equally on images presented for direct comparison. No other image processing was used. No quantifications or substantive comparisons were based on these images.

Three-dimensional (3D) object analysis

The number, volume, and internal density of puncta were calculated using the 3D Objects Counter function of ImageJ. Puncta greater than 3 standard deviations above the average puncta volume were excluded from the analysis in order to minimize the contribution of lipofuscin granules, which often stain non-specifically.

Colocalization analysis

The overlap in fluorescence between two aligned TIFF stacks was calculated as previously described (Micheva et al., 2010a). This methodology is based on the van Steensel method (van Steensel et al., 1996). Briefly, we computed a three-dimensional normalized cross-correlogram from a $20 \times 20 \times 6.3\ \mu m^3$ volume of neuropil for each pair of antibodies for a range of lateral offsets approximating the size of a synapse. Pairs of antibodies with nonrandom associations (either positive or negative) should demonstrate a nonzero correlation effect that asymptotically approaches 0 at offset ranges exceeding their scale of interaction. For pairs of antibodies showing nonrandom associations based on the van Steensel method, we created new image stacks representing all areas of overlap in fluorescence between the two antibodies of interest using the “Image Calculator” and “Multiply” functions in ImageJ. The total number of puncta, as well as the volume and internal density of puncta, in this new image stack was then calculated using the “3D Objects Counter” function of ImageJ. In order to normalize the change in colocalization in Ts65Dn mice to the total number of puncta in each channel, an expected colocalization between two antibodies was calculated by expressing the total number of puncta for each antibody as a percentage of 2N values, then calculating the average of these percent 2N values for the two colocalized antibodies. For this analysis, the overlap of the two channels was defined such that puncta that were closely apposed were considered to be colocalized. Thus, the area of the cell body surrounding the DAPI-stained nucleus are included in the pTrkB and DAPI colocalization; and the entire synapse, including both the presynaptic compartment and postsynaptic density, are included in the pTrkB and synapsin-1 colocalization

Synapse classification

For each synapse class of interest, 300–500 randomly selected synapses were classified manually using synaptograms (Micheva et al., 2010a). In order to be classified as a synapse, the synaptogram was required to meet the following criteria: All synapse subtypes were required to contain synapsin-1 staining in at least 2 consecutive sections. Glutamatergic synapses were required to contain VGluT1 or VGluT2 staining in at least 2 consecutive sections and PSD95 staining, overlapping with VGluT1 or VGluT2, in at least 1 section. GABAergic synapses were required to contain GAD and VGaT staining in at least 2 consecutive sections and gephyrin, overlapping with VGaT or GAD, in at least 1 section. Cholinergic synapses were required to contain either VAChT or ChAT staining in at least 2

consecutive sections. for automated synapse classification, the list of manually-classified synapses with their associated feature vectors were fed into a Random Forest Ensemble machine learning algorithm capable of extrapolating the given classification parameters to each potential synapse in the entire volume with some estimable error rate (6–12%, depending on the synapse class). The puncta features used for this analysis were the integrated brightness, center of mass, moment of inertia, and local brightness of puncta from each antibody in the antibody panel that were located within 1μm of the synapsin-1 punctum. Next, all synapsin-1 puncta in the volume (80,000–150,000 puncta, depending on the size and number of sections in the volume) and their associated features were extracted, and the same algorithm was used to classify synapses of each specified sub-class within the entire volume.

Antibodies

For Western blot, primary antibodies directed against TrkA, pTrkA, EGFR, pERK, ERK, pAKT, AKT, pPLCγ, PLCγ, pMEK1/2 (Cell Signaling Technology, Danvers, MA); TrkB (BD Biosciences, San Jose, CA), pTrkB (AbCam, Cambridge, MA), BDNF (Alamone Labs, Jerusalem, Israel and Santa Cruz Biotechnology, Santa Cruz, CA) and β-actin (Sigma-Aldrich, St. Louis, MO) were used. For AT, we used the above listed antibodies, plus antibodies against α-Tubulin (Abcam); synapsin-1, VGluT1, VGluT2, GAD, ChAT (Millipore, Billerica, MA); VGaT, VAChT (Synaptic Systems, Goettingen, Germany); Rab5 (Millipore and Santa Cruz) and PSD95 (Neuromabs, Davis, CA). Secondary antibodies for immunohistochemistry were highly preadsorbed mouse, rabbit, goat, or guinea pig IgGs conjugated to Alexa Fluor 488, 594, and 647 (Invitrogen) used at a dilution 1:150. The coverslips with sections were mounted using SlowFade Gold antifade with DAPI (Invitrogen, Carlsbad CA). To elute the applied antibodies, the mounting medium was washed away with distilled water and a solution of 0.2 M NaOH and 0.02% SDS in distilled water was applied for 10 minutes. After an extensive wash with Tris buffer and distilled water, the coverslips were dried and placed on a hot plate (60°C) for 30 minutes. To confirm that antibodies were completely eluted, a subset of arrays was eluted, incubated with blocking solution alone (0.05% Tween and 0.1% BSA in Tris) in the absence of primary antibody, followed by incubation with a secondary antibody and section mounting and imaging.

The specificity and reliability of antibodies were tested previously for the majority of antibodies used (Micheva et al., 2010a). Additional antibodies were validated either by staining simultaneously with two different antibodies raised in different host animals against the same antigen and confirming a similar staining pattern (Rab5, VAChT), comparing the staining pattern of the test antibody to an antibody with similar distribution (e.g. VAChT and ChAT, TrkB and pTrkB, pERK and ERK, pAKT and AKT), or comparing the staining pattern in LR white ultrathin sections to those from conventional immunohistochemistry (for TrkA, TrkB, and pTrkB). For the pTrkB antibody, the pattern of staining seen in LR white ultrathin sections was similar to that seen in an earlier study (Chen et al., 2010). To further confirm the specificity of this antibody, we restained the same ribbon with the pTrkB antibody on multiplex cycle 1 and 7 and compared the staining pattern by overlaying the two images. We found over 90% concordance between the two staining sessions. Since different

antibodies are know to have different off-rates in LR white fixed tissue (Micheva et al., 2010a), we imaged all arrays immediately after staining. In order to control for variability between individual staining sessions, a distinct pair of samples (a 2N and a Ts65Dn sample) were stained and imaged simultaneously, and all quantitative analyses were performed by comparing the ratio of values between the pair. To limit the effect of variability of off-rates on staining differences within a single imaging session, we alternated the order in which a pair (one 2N and one Ts65Dn) of arrays was imaged in each experiment.

Results

Increased TrkB signaling in Ts65Dn cortical synaptosomes

Given widespread changes in early endosome structure, the known retrograde trafficking of NTFs and their activated receptors in early endosomes, and the reduced NTF retrograde transport in Ts65Dn mice (Cataldo et al., 2003; Deinhardt et al., 2006; Grimes et al., 1996; Salehi et al., 2006; Valdez et al., 2005), we hypothesized that increased NTF signaling would be present in synapses. We examined Trk signaling in cortical synaptosomes prepared from 2N and Ts65Dn mice in order to study signaling in an isolated synaptic compartment that retains physiological signaling capacity (see Fig 1). We found a significant increase in the level of phosphorylated TrkB (pTrkB) in Ts65Dn samples (Fig. 2A and B). Surprisingly, we also found a significant increase in total TrkB. Indeed, there was a trend towards a higher ratio of total TrkB to pTrkB in Ts65Dn mice; however, the difference was not significant (4.11 ± 0.54 in Ts65Dn versus 3.05 ± 0.23 in 2N, $p = 0.093$, $n = 8$ per genotype). The TrkB antibody recognizes several glycosylated forms of the full-length TrkB protein, as well as the truncated (95kDa) form of TrkB, which lacks the catalytic intracellular domain necessary for downstream signaling (Andero et al., 2011; Autio et al., 2011; Fletcher et al., 2008; Huang and McNamara, 2012; Klein et al., 1990). There was a significant increase in the band density of all forms of TrkB in cortex in Ts65Dn mice, although the most dramatic was observed in the two glycoproteins with the highest molecular weights, gp160 and gp148 for which levels the Ts65Dn samples were 5-fold those in 2N samples (Fig. 2A and B).

To determine whether the increases in total TrkB and pTrkB were unique to this receptor, we measured the levels of both the highly homologous tyrosine receptor kinase TrkA, and epidermal growth factor receptor (EGFR), a member the Erb2 family of receptor tyrosine kinases whose signaling and trafficking differ from that of the Trk receptors (Oda et al., 2005). No significant difference in levels of TrkA or EGFR was detected between 2N and Ts65Dn synaptosomes (Fig. 2A, B). In addition, there was no significant difference in levels of the phosphorylated form of TrkA (Ts65Dn = $97.40 \pm 4.59\%$ of 2N, $p = 0.69$). Thus, while we cannot rule out increases in signaling and trafficking of other receptors in Ts65Dn cortex, these findings point to increases in TrkB that are marked and possibly distinctive.

Phosphorylation of TrkB by BDNF leads to downstream activation of multiple signaling pathways, including those mediated by Ras/MAPK, PI3K, and PLCγ (Knusel et al., 1992; Zirrgiebel et al., 1995). To determine whether or not increased TrkB activation was correlated with increases in downstream signaling pathways, total and phosphorylated levels of Ras/MAPK pathway proteins MEK1/2 and ERK, the PI3K protein AKT, and the PLC pathway proteins PLCγ1 and PLCγ2 were measured in synaptosomes by immunoblotting

with antibodies specific for total and phosphorylated forms of these proteins. As compared to 2N synaptosomes, Ts65Dn synaptosomes exhibited increases in phospho-MEK1/2, phospho-ERK and phospho-AKT; there was no increase in the level of phosphorylated forms of PLCγ1 or in the levels total ERK1/2, total AKT, or total PLCγ1 (Fig. 2A and 2C). The greatest increase was for activated MEK1/2 where levels were more than 3-fold those in 2N samples. pERK and pAKT levels were 2-fold the 2N value.

We conclude that Ts65Dn cortical synaptosomes demonstrate marked increases in total TrkB, activated TrkB and a subset of downstream signaling pathways, consistent with increased activation and signaling of this receptor to its downstream targets.

Increased TrkB signaling in Ts65Dn somatosensory cortex

TrkB signaling is relevant to the structure and function of a number of cortical neurons and the circuits in which they participate (Xu et al., 2000). To confirm increases in TrkB signaling in the Ts65Dn cortex, and to define the locus of these increases, we undertook studies to define the synapse types and sub-cellular compartments that contain TrkB signaling. We used AT, a method that makes it possible to carry out proteomic analysis at the single synapse level of resolution (Micheva et al., 2010a; Micheva and Smith, 2007). Cortical arrays from layers 2/3, 4, and 5a somatosensory cortex were sequentially immunostained with antibodies against TrkB, pTrkB, downstream signaling molecules activated by TrkB, markers of specific sub-cellular compartments, and a panel of synaptic antibodies.

Volume renderings from 2N and Ts65Dn cortical arrays showed that pTrkB staining was primarily confined to the neuropil and that it was excluded from nuclei (Fig. 3A and B). While all signaling markers studied exhibited a punctate staining pattern, pTrkB, pERK, and pAKT positive puncta were often arranged in an apparent “beads on a string” pattern, consistent with localization in a neuronal process (Nikolaev et al., 2009) (Fig. 3B). The staining pattern raised the possibility that TrkB-positive signaling endosomes were being imaged near axon terminals; accordingly, we undertook additional colocalization analyses to define subcellular localization.

AT analysis of cortical arrays confirmed the increase in TrkB and TrkB-mediated signaling found in Ts65Dn synaptosomes. There was an increase in the number of puncta positive for total TrkB in layers 2/3 and 4, but not in layer 5a (Fig. 3B and D). In layers 2/3 and 5a, Ts65Dn mice showed a significant increase in the number of puncta positive for pTrkB (Fig. 3B and D). On the other hand, for pERK1/2 and pAKT, there was a significant increase in puncta number only in layers 4 and 5a. Interestingly, there was a strong but insignificant trend towards a decrease in pERK and pAKT positive puncta in layers 2/3 (Fig 3B and D). The staining pattern of the early endosome marker Rab5 showed a significant increase in the number of puncta in layer 5a, with no increase in layers 2/3 and 4 (Fig. 3B and D). The increase in the number of Rab5 puncta in layer 5a was strikingly almost 4-fold that in the 2N cortex. As in the cortical synaptosome studies, there was no increase in the number of pPLCγ positive puncta in any layer (data not shown). In addition to counting puncta for each of the markers, we also measured puncta volume. Ts65Dn cortices exhibited a significant shift in volume towards larger puncta for all markers except total TrkB (Fig. 3C). In

summary, the data confirm the finding of increased TrkB signaling, and provide the additional insight that increases in TrkB signaling and downstream signaling markers differ across cortical sub-domains, as reflected in the distinct ratios to 2N values for total TrkB, pTrkB, pERK, pAKT, and Rab5 puncta in each cortical layer.

Changes in the sub-cellular localization of pTrkB in Ts65Dn somatosensory cortex

The marked increase in TrkB and related signaling proteins observed in layer 4 in Ts65Dn mice, prompted an in-depth analysis of this cortical layer. To assess the sub-cellular distribution of pTrkB, we first measured the colocalization of pTrkB with several markers of sub-cellular compartments in cortical arrays from 2N and Ts65Dn mice (Fig. 4). The relative amount of pTrkB present in different sub-cellular compartments was quantified by measuring pTrkB colocalization with DAPI (cell body), α-tubulin (neuronal processes), and synapsin-1 (synapses). In 2N mice, pTrkB was most frequently colocalized with α-tubulin (11.53 ± 0.60%), followed by DAPI (7.16 ± 2.27%) and synapsin-1 (7.85 ± 0.26%) (Table 1). Thus, about 27% of pTrkB was localized with the combination of these markers. The same analysis was conducted for the Ts65Dn cortex. We found that increased pTrkB was disproportionally localized to synapses, as evidenced by a significant increase in the number of puncta positive for pTrkB that colocalized with the synaptic marker synapsin-1 (Fig. 4E, K, and M). There was also a significant increase in the number of pTrkB and α-tubulin positive puncta (Fig. 4F, L, and M), suggesting an increase in pTrkB in neuronal processes. Colocalization of pTrkB and Rab5 positive puncta was also significantly increased (Fig. 4D, J, and M). While there was no change in the amount of pTrkB colocalization with DAPI, the relative percentage of total pTrkB staining present in cell bodies can also be estimated by considering the amount of pTrkB present in this compartment as compared with the other compartments. While in the 2N cortex staining for all compartments measured 27%, in Ts65Dn it was 62%. Calculating the ratio of pTrkB staining in cell bodies with respect to all three compartments shows a decrease from 27% in 2N cortex to 19% in Ts65Dn. In summary, AT analysis of the sub-cellular location of pTrkB in Ts65Dn somatosensory cortex reveals an increase in activated TrkB at synapses and in neuronal processes. The data are evidence for increases in TrkB signaling and for differential subcellular distribution of the markers for this signaling pathway in cortical neurons that points to increases in synapses and processes and decreases in neuronal somas.

Compartmentalization of pTrkB and downstream signaling in early endosomes in the 2N and Ts65Dn somatosensory cortex

Because enlargement of early endosomes are characteristic of both DS and the Ts65Dn mouse, and because early endosomes retrogradely transport BDNF/TrkB signaling complexes, we asked whether or not increases in TrkB signaling in Ts65Dn were present in early endosomes. We examined in cortical volumes the extent to which pTrkB and its downstream targets pERK and pAKT were colocalized with Rab5, a marker of signaling endosomes in cortex. Colocalization of pTrkB with both pERK (Fig. 4B, H, and M) and pAKT (Fig. 4C, I, and M) was significantly increased in Ts65Dn mice. The overall 1.5-3 fold increase in pTrkB, pERK, and pAKT puncta in Ts65Dn mice over 2N values (Fig. 3) is highly significant. However, it underestimates considerably the dramatically increased colocalization between these proteins. In fact, when colocalization of pTrkB with other

markers was normalized to take into account the overall increase in number of pTrkB puncta, pTrkB colocalization with pERK was over 3 fold higher in Ts65Dn mice compared to 2N; colocalization of pTrkB and pAKT was increased over 2 fold (Fig. 4M). In addition, there was a significant increase in both the total number of Rab5 positive puncta and the colocalization of pTrkB with Rab5 (Fig. 4D, J, and M).

The antibody multiplexing capacity of AT allowed us to visualize signaling endosomes in cortical arrays, defined by the colocalization of pTrkB, pERK or pAKT, and Rab5: this analysis showed an increase in the number of early endosomes containing activated TrkB and downstream signaling molecules in Ts65Dn cortex (Fig. 4A–K). This analysis further substantiates increased activation of TrkB in Ts65Dn cortex and indicates that it is reflected in an increase in the number of pTrkB positive signaling endosomes.

Increased TrkB signaling in pre- and postsynaptic compartments in Ts65Dn cortex

To define the subclass(es) of synapses in which TrkB signaling is present, and to determine which are impacted by increases in pTrkB in the Ts65Dn cortex, we measured the extent to which pTrkB was colocalized with a panel of pre- and postsynaptic markers. Colocalization of pTrkB with synaptic markers in 2N mice varied from 0.35 ± 0.01% with the presynaptic cholinergic marker VAChT to 4.19 ± 0.39% with the glutamatergic presynaptic marker VGluT1 (Table 2). Representative volume renderings from 2N and Ts65Dn mice cortex layer 4 show a GFP positive apical dendrite from a layer 5 pyramidal cell, as well as all synapsin-1 positive puncta (Fig. 5A and D). The Ts65Dn cortex showed a significant increase in the total number of VGaT positive puncta and a significant decrease in the total number of PSD95 positive puncta (Fig. 5 E–G). Comparing colocalization of pTrkB with markers of specific synapse subtypes in 2N and Ts65Dn mice, we found that the Ts65Dn cortex exhibited significant marked increases of pTrkB with the presynaptic GABAergic marker VGaT, with the postsynaptic GABAergic marker gephyrin, and the postsynaptic glutamatergic marker PSD95 (Fig. 5E–G). In comparison to the 2N cortex, colocalization with VGaT was 2-fold normal; the values for gephyrin and PSD95 were 4-fold the 2N level. When normalized by the number of these synaptic markers in Ts65Dn cortex, increased colocalization of pTrkB with gephyrin and PSD95 approximated 8-fold (Fig. 5G). In contrast, pTrkB was much less frequently colocalized with the presynaptic glutamatergic marker VGluT1/2, although this did not reach statistical significance due to variability. We conclude that increased TrkB signaling is present in both GABAergic and glutamatergic synapses; with respect to GABAergic synapses, the increases are registered in both the pre- and postsynaptic compartments.

Examining pTrkB in individual GABAergic synapses

The GABAergic synapses onto apical dendrites of layer 5 pyramidal cells are likely to arise from GABAergic interneurons in the same cortical layer, such as basket, bipolar, multipolar, and neurogliaform interneuron subtypes (Thomson and Lamy, 2007). The majority of glutamatergic synapses containing pTrkB on layer 4 dendritic spines of layer 5 pyramidal neurons are VGluT2 positive (data not shown), suggesting that they are synapses made by thalamocortical projections (Micheva et al., 2010a).

To explore further the increases in pTrkB at individual GABAergic synapses, we examined the apical dendrites of layer 5 pyramidal cells and identified GABAergic synapses on GFP positive dendritic spines in layer 4 (Fig. 6A and F). High magnification volume renderings from 2N (Fig. 6A–E) and Ts65Dn (Fig. 6F–J) cortical layer 4 were examined using several pre- and postsynaptic markers specific to GABAergic synapses. While pTrkB positive and pTrkB negative GABAergic synapses were found in both the 2N and Ts65Dn cortex, in the Ts65Dn cortex there was a greater proportion of pTrkB positive GABAergic synapses (Fig. 6F–J). pTrkB positive puncta were most often seen overlapping the postsynaptic GABAergic marker gephyrin (Fig. 6E and J), in close apposition to the presynaptic markers VGaT and GAD (Fig. 6C, D, H, I), consistent with the preceding analysis in volume renderings showing increased pTrkB associated with gephyrin (Fig. 5E). This high resolution, single layer analysis of pTrkB, demonstrates that the activated receptor is present in specific sub-synaptic compartments, including the pre- and postsynaptic compartments of GABAergic synapses and presynaptic GABAergic elements in contact with the dendrites of cortical neurons.

Synapse classification in 2N and Ts65Dn mice

Increased colocalization of pTrkB with specific synaptic markers and phosphorylated downstream signaling molecules raises the possibility that synapse subtypes may be differently impacted. The analysis of pTrkB colocalization with single synaptic and signaling markers allowed us to determine the sub-cellular compartment(s) in which TrkB signaling was increased in the Ts65Dn cortex, but to precisely analyze synapse subtypes in 2N and Ts65Dn we required a method that allows for classifying synapses via the simultaneous presence of multiple markers. To make this possible, we generated synaptograms - visualizations that display immunofluorescence data for multiple antigens and are therefore useful for analyzing multi-channel volumetric image data (Micheva et al., 2010a) (Fig. 7A). 300–500 synaptograms were manually classified into glutamatergic, GABAergic, or cholinergic based on the presence of subtype specific markers (see Experimental procedures). In addition, synapses were classified as positive or negative for pTrkB, Rab5, pERK, and pAKT.

Next, a machine learning algorithm was used to classify over 100,000 synapses per data set based on the manual synapse classification. The number of synapses belonging to each synapse subclass was quantified in 2N and Ts65Dn data sets (Fig. 7B). There was no difference in the total number of synapses in 2N and Ts65Dn mice, but Ts65Dn mice showed a significant ∼ 50% increase in the total number of pTrkB positive synapses, a significant increase in the number of GABAergic synapses, and significantly-fewer glutamatergic and cholinergic synapses (Fig 7B). Accounting for the decrease in total glutamatergic synapses, the relative increase in pTrkB-containing glutamatergic synapses was 2-fold that in 2N. We conclude that increases in TrkB signaling impact a number of different synapse types with the most marked deviations from 2N present in inhibitory synapses.

Localization of TrkB receptors in cortical synaptosomes from 2N and Ts65Dn mice

To explain increased TrkB synaptic signaling in the Ts65Dn cortex, we envisioned several possibilities: increased expression of TrkB, increased expression or protein levels of BDNF, increased access of BDNF to TrkB, decreased retrograde trafficking of TrkB-positive endosomes, or decreased downregulation of activated TrkB. To test the possibility that increased gene expression of TrkB was responsible, we measured TrkB mRNA levels in 2N and Ts65Dn cortex and found no significant difference (Ts65Dn = 121.68 ± 5.48% of 2N, $p = 0.12$). To ask if increased expression of the TrkB ligand BDNF might contribute to increased signaling, we also measured the level of BDNF mRNA and found no difference (Ts65Dn = 90.48 ± 8.78% of 2N, $p = 0.36$). Finally, we compared the amount of BDNF protein in 2N and Ts65Dn cortex. We found a trend towards lower levels of BDNF in Ts65Dn mice, although the difference did not reach statistical significance (Ts65Dn = 65.99 ± 17% of 2N, $p = 0.07$). Thus, the increase in TrkB and related proteins is not due to increased expression of the genes for TrkB or BDNF.

Next we examined the possibility that BDNF binding to increased surface levels of TrkB was responsible. To examine this we carried out studies of surface binding of Quantum dot labeled BDNF (QD-BDNF) in 2N and Ts65Dn cortical synaptosomes. Rather than the predicted increase in surface binding, QD-BDNF binding was significantly decreased in Ts65Dn synaptosomes (Fig. 8A, C, E). There was very little surface binding of QD alone (QD-veh) in either 2N or Ts65Dn synaptosomes (Fig. 8B, D, and E), confirming that the surface binding observed is specific and receptor-mediated.

Decreased surface binding of BDNF in Ts65Dn mice suggested that synaptosomes from Ts65Dn mice would respond less robustly to exogenous BDNF. To test this idea we treated cortical synaptosomes with BDNF and measured pTrkB, pERK, and pAKT. Treatment of 2N synaptosomes with BDNF elicited a significant increase in pTrkB, pERK, and pAKT (Fig. 9A and B). However, in Ts65Dn synaptosomes, BDNF treatment had no significant effect on levels of pTrkB, pERK, or pAKT (Fig. 9A and C). BDNF failed to induce a response in Ts65DN synaptosomes despite the fact that BDNF was able to bind to surface receptors (Fig 8), albeit at reduced levels. With vehicle treatment, as predicated, BDNF elicited a more robust response in Ts65Dn synaptosomes than in 2N synaptosomes (Fig 9).

We conclude that significant changes in TrkB trafficking and signaling are present in the cortex of Ts65Dn mice. Increased levels of signaling in Ts65Dn cortical synaptosomes with vehicle treatment, and the severely blunted response to BDNF, combine with the surface binding studies to document these changes. The data are further evidence that TrkB and pTrkB are located in internal membranes. The studies reported above point to early endosomes as one locus of excessively active downstream signaling proteins. The data for the marked disconnect between BDNF responsiveness and TrkB activation in the Ts65Dn cortex suggest that dysregulation of BDNF/TrkB signaling may disrupt normal synaptic function as well as synaptic responses to BDNF in the Ts65Dn cortex.

Discussion

In this study we used a combination of biochemistry and AT to identify a marked increase in TrkB activation in the cortex of Ts65Dn mice and to pinpoint the sub-cellular loci of TrkB signaling abnormalities. We found increased TrkB activation as well as increased activation of the MAPK and PI3K signaling pathways in cortical synaptosomes and showed that these changes could be traced to signaling endosomes and to both the pre-and postsynaptic compartments of GABAergic synapses, as well as the postsynaptic compartment of glutamatergic synapses. AT analysis revealed that changes in the activation of TrkB and other signaling markers differed by layer, pointing to differences in cortical sub-domains that likely reflect differences in the cellular elements present and the synapses present. Increased TrkB signaling was not due to increased levels of the receptor or its ligand, or to differences in access of BDNF to TrkB. In fact, surface TrkB receptors were significantly decreased and the response of synaptosomes to exogenous BDNF was blunted in Ts65Dn synaptosomes. Instead, the data are evidence for increased TrkB and pTrkB in internal membranes; early endosomes are a likely locus on the basis of the increased colocalization of pTrkB, pERK, pAKT , and Rab5. Taken together, the findings are evidence of dysregulation of BDNF/TrkB signaling and trafficking, and to the existence of synapses in which TrkB signaling is not responsive to its ligand. These changes can readily be envisioned as impacting the function of cortical circuits in Ts65Dn mice and cognitive functions in which they participate.

A number of previous studies support the view that changes in NTF signaling are present in DS and other neurodegenerative disorders (Ahmed et al., 2013; Ahmed et al., 2012). One line of investigation links changes in signaling to a decrease in NTF retrograde axonal transport within the endosomal system, with resulting dysfunction and degeneration of dependent cell bodies (Cataldo et al., 2003; Cooper et al., 2001b; Salehi et al., 2006). In another, increased levels of truncated TrkB receptor, hyperphosphorylation of the AKT-mTOR pathway, and a loss of responsiveness to BDNF was found in the hippocampus of DS model mice (Dorsey et al., 2002; Troca-Marin et al., 2011). Past studies, complemented by those reported here, demonstrate that changes in TrkB signaling are present in multiple brain regions in DS mouse models and, possibly in human DS. Our data support the hypothesis that increased activation of TrkB signaling is linked to changes in endosomal trafficking of the receptor.

We found that changes in cortical pTrkB and downstream signaling markers were specific to cortical layers and to synaptic subtypes. Though increased activation of TrkB signaling was present in all cortical layers studied, increased activation of downstream signaling was seen only in layers 4 and 5a. In fact, we saw a trend towards decreased downstream signaling in layer 2/3. The differences in layers may be due to differential BDNF/TrkB signaling in different neuronal subtypes in the cortex. In the case of neurons that form synapses within the same cortical layer as their soma, activated downstream signaling molecules in synapses, within axons, and those retrogradely transported to cell bodies would all be included in the measurements within a single cortical layer. In contrast, for neurons that send axons to different cortical layers, signaling at the synapse and distal axons is spatially distant from signaling in proximal axons and in the cell body. The increase in pTrkB seen in all layers,

including increases in specific synaptic subtypes in layer 4, suggests that this change is present in both interneurons and neurons whose axons project to different cortical layers and to loci outside the somatosensory cortex. The absence of increased activated downstream signaling markers in layers 2/3 may be explained by reduced activation by pTrkB within this level or to decreased transport in endosomes with TrkB from other layers, possibly from synapses in layers 4 and 5a. Additional AT analyses that includes antibodies specific to subpopulations of glutamatergic and GABAergic synapses will be needed to shed light on the mechanisms and processes that underlie the layer-specific changes observed.

We observed an increase in pTrkB both presynaptically and postsynaptically in GABAergic synapses, a synaptic subclass known to be abnormal in Ts65Dn mice. Previous studies of Ts65Dn mice have identified increased $GABA_A$ and $GABA_B$ receptor-mediated inhibition in hippocampus along with loss of LTP in CA3 and dentate gyrus (Belichenko et al., 2009b; Kleschevnikov et al., 2004; Siarey et al., 1997), as well as an increase in the localization of VGaT and GAD65 at GABAergic synapses (Belichenko et al., 2009a; Belichenko et al., 2009b). Furthermore, Ts65Dn hippocampal and cortical synaptosomes exhibit increased stimulus-evoked release of GABA (Begenisic et al., 2011). It has been suggested that abnormal excitatory/inhibitory balance may contribute to learning and memory deficits in these mice, in DS, and in other neurodegenerative disorders such as AD (Rissman and Mobley, 2011).

We propose that the increased TrkB signaling reported here could contribute to excessive inhibition in Ts65Dn mice by influencing the development of cortical inhibitory circuits and by increasing GABA release and signaling. BDNF/TrkB signaling is known to affect the development and maintenance of GABAergic synapses in many different brain areas, including the cerebellum (Chen et al., 2011a; Rico et al., 2002; Seil and Drake-Baumann, 2000), hippocampus (Yamada et al., 2002), and cerebral cortex (Itami et al., 2003; Itami et al., 2007; Jiao et al., 2011; Lush et al., 2005; Patz et al., 2003; Sanchez-Huertas and Rico, 2011). Supporting the suggestion that increased TrkB signaling contributes to increased inhibition, we found an increase in the number of GABAergic synapses in Ts65Dn mice, as well as a marked increase in GABAergic synapses containing activated TrkB, in layer 4 somatosensory cortex, the layer in which we chose to focus our examination. Thus, there was a change in this layer in the ratio of excitatory to inhibitory synapses as well as increased activation of TrkB and downstream signaling molecules.

Increased colocalization of pTrkB with PSD95, a postsynaptic scaffolding protein component of excitatory synapses, was of interest in light of earlier findings showing that BDNF/TrkB signaling recruits PSD95 to NMDAR positive postsynaptic sites via the PI3K pathway (Yoshii and Constantine-Paton, 2007). However, we observed a decrease in both the number of PSD95 puncta and glutamatergic synapses. How could excessive TrkB signaling lead to both an increase in GABAergic synapses and a decrease in glutamatergic synapses, when TrkB is involved in the function of both synapse subtypes? One explanation is that changes in endosomal trafficking of TrkB, could both increase TrkB activation in synapses and decrease retrograde axonal transport of TrkB signaling endosomes to neuronal cell bodies. Evidence to support changes in endosomal trafficking in prior studies includes: 1) Increased Rab5 staining on enlarged endosomes in human DS and mouse tissue (Cataldo

et al., 2000; 2003); 2) the presence of NGF within enlarged Rab 5 endosomes in cholinergic axons in the Ts65Dn hippocampus (Salehi et al., 2006); 3) a small but significant increase in endocytosis of NGF added to Ts65Dn hippocampal synaptosomes (Cooper et al., 2001a); and 4) failure to properly transport NGF from the hippocampus to basal forebrain in these mice (Cooper et al., 2001a; Salehi et al., 2006).

The current study gives further evidence for changes in endosomal function and trafficking in the Ts65Dn cortex: 1) there is a large increase in the amount of both TrkB and pTrkB in synaptosomal membranes; 2) pTrkB shows increased colocalization with Rab5 positive endosomes; and 3) while the distribution of pTrkB is increased at synapses it is decreased in neuron cell bodies. The presence of changes in endosomal function and trafficking are compelling. To what extent they explain selective effects on GABAergic and glutamatergic synapses in the Ts65Dn cortex is unknown, but it is possible that changes in synaptic and retrograde transport of BDNF/TrkB signals differentially impacts inhibitory interneurons, whose axons are short versus pyramidal neurons whose signals are carried much longer distances from synapses in cortex and from subcortical regions. For glutamatergic axons making longer-range connections, the transport deficit may more severely compromise the delivery of TrkB-mediated signals to the cell soma. The decrease in cholinergic synapses we found supports this hypothesis, since these terminals arise from projecting axons originating in the nucleus basalis of Meynert of the basal forebrain (Hohmann et al., 1991).

Ts65Dn cortical synaptosomes showed a blunted response to BDNF. The mechanism is unknown, but we speculate that the TrkB signaling pathway is constitutively active at a higher level compared to in 2N mice. We propose that the high level of TrkB signaling intracellularly in synapses, along with the blunted response to exogenous BDNF, contributes to a “runaway synapse” phenotype in Ts65Dn cortex, characterized by a high level of constitutive activity in the BDNF/TrkB signaling pathway and, subsequently, an inability to modulate synaptic strength and activity in response to BDNF. The excessive TrkB signaling in Ts65Dn cortex described herein may contribute to the increased inhibition and loss of synaptic plasticity in the Ts65Dn mouse model of DS and may underlie some of the cognitive abnormalities present in humans with DS and those with AD.

The increases in TrkB, pTrkB and the signaling pathways they engage, as well as the distribution of these markers, prompts consideration of their possible effects on cortical function. Since the BDNF/TrkB signaling pathway is implicated in synapse development and maintenance, the changes in TrkB may be a source of changes in the structure and function of synapses in Ts65Dn mice. Excessive TrkB signaling may affect cortical development and, perhaps more importantly, synaptic plasticity in the adult brain (Gorski et al., 2003; Itami et al., 2003; Kang and Schuman, 1995). In fact, an emerging role for inhibitory cortical circuits in modulating synaptic plasticity supports the idea that over-inhibition during both development and adulthood play a critical role in deficient synaptic plasticity (Chen et al., 2011b), a phenomenon that may apply to cortical synaptic plasticity in Ts65Dn mice. Thus, it is possible that increased TrkB signaling intracellularly in synapses, together with the blunted response to exogenous BDNF, both contribute to an inability of cortical neurons to modulate synaptic strength and activity in response to BDNF. Studies examining what role, if any, TrkB activation may play in modifying excitatory and

inhibitory neurotransmission in Ts65Dn mice can now be initiated to elucidate the mechanism(s) involved.

The mechanism underlying the increased activation of the TrkB signaling pathway in Ts65Dn mice is yet to be defined. Attention can now be focused on endocytosis, recycling and trafficking of these receptors. Since increased gene dose for APP has been shown to be both necessary and sufficient for disrupting retrograde axonal transport of NGF in mouse models of DS, examining what role for APP may play in changes in endocytosis and trafficking are warranted. Likewise, the functional consequences of increased TrkB signaling is far from clear. Because the increase in GABAergic transmission impacted both inhibitory and excitatory synapses it is uncertain as to how circuit properties and processing would change. However, we can speculate that excessive TrkB signaling may lead to increased GABA release, a phenomenon that has been observed in cortical and hippocampal synaptosomes and cortical slices from Ts65Dn mice(Begenisic et al., 2014; Kleschevnikov et al., 2012a; Mitra et al., 2012).

An important consideration is whether the changes in TrkB signaling are primary, or instead represent a secondary, compensatory response to another process. Increased TrkB signaling might increase activity of GABAergic synapses, causing cortical circuits to adapt by increasing the size of active zones of glutamergic synapses to preserve activity. This idea supported by the earlier finding of selective enlargement of asymmetric synapses in the Ts65DN cortex (Belichenko et al., 2004), and additional evidence of similar compensatory reactions (Yin and Yuan, 2014). However we currently have no evidence that this is the case, or that changes in GABAergic synaptic function are directly linked to increased TrkB signaling. To distinguish between primary and compensatory effects will require studies to define the underlying gene(s) and mechanisms that underlie cortical circuit development and homeostasis in models of DS.

Although this study provides new insights into TrkB signaling in the Ts65Dn cortex, there are a number of limitations. First, the biochemical findings in synaptosomes used 3–6 month old mice, whereas AT was done in 12 month old mice, raising the question as to whether the results for TrkB signaling were consistent across age. We chose older animals for AT because Ts65Dn mice show progressive neurodegeneration, including degeneration of locus coereleus and basal forebrain by 12 months (Salehi 2006 and 2009), so at this age cortical abnormalities are more likely to be detected. On the other hand, it was not possible to make synaptosome preps from 12 month old mice due to technical limitations. We addressed the age discrepancy in the following ways: 1) Most important is that despite the use of different techniques at different ages, we found very similar patterns and increases in TrkB signaling; 2) Given the inability to make high quality synaptosomal preps in older mice, we examined whole cortical extracts from 12 month old mice and demonstrated the same trends in signaling differences. While the differences between 2N and Ts65Dn did not reach statistical significance for most signaling proteins (Supplemental Figure 1), this was expected given the “dilution” by the presence of the tissue comprising the entire cortex versus the “concentration” of signal in isolated synapses. Indeed, AT findings document the probability of signal dilution in view of the fact that changes in TrkB signaling pathways were not uniformly increased across all cortical layers; 3) Finally, we confirmed findings using AT by

performing several different types of analyses using this technique. Taken together, the data support our interpretation of significant differences in TrkB signaling in the Ts65Dn cortex.

Another limitation is our inability to distinguish subtypes of GABAergic synapses, a technical limitation of AT that limits our ability to identify which subpopulations of inhibitory synapses were affected. A more detailed AT analysis of synaptic subpopulations is needed to provide a clearer understanding as to which neurons are affected in the Ts65Dn cortex, what changes characterize their synaptic relationships, and whether or not changes in synaptic fine structure are present. It will then be possible to define more clearly what role is played by increased TrkB activity on inhibitory transmission in the Ts65Dn mouse. Finally, because the AT ribbon is comprised of a very small slice of cortical tissue, the selection process could mask differences unique to specific cortical regions. In this respect, the biochemical studies are useful in providing support to the view that the changes documented do characterize more generally the status of TrkB signaling. Nevertheless, exploration of possible regional differences are warranted to more fully define changes in cortex and other brain regions in mouse models of DS.

Supplementary Material

Refer to Web version on PubMed Central for supplementary material.

Acknowledgements

This work was funded by grants from the Larry L. Hillblom Foundation, the NIH-NINDS (NS024054, NS066072), the LuMind Foundation (formerly, the Down Syndrome Research and Treatment Foundation), Research Down Syndrome, the Alzheimer's Association and the LeJeune Foundation.

References

Ahmed MM, Dhanasekaran AR, Tong S, Wiseman FK, Fisher EM, Tybulewicz VL, Gardiner KJ. Protein profiles in Tc1 mice implicate novel pathway perturbations in the Down syndrome brain. Human molecular genetics. 2013; 22:1709–1724. [PubMed: 23349361]

Ahmed MM, Sturgeon X, Ellison M, Davisson MT, Gardiner KJ. Loss of correlations among proteins in brains of the Ts65Dn mouse model of down syndrome. Journal of proteome research. 2012; 11:1251–1263. [PubMed: 22214338]

Andero R, Heldt SA, Ye K, Liu X, Armario A, Ressler KJ. Effect of 7,8-dihydroxyflavone, a small-molecule TrkB agonist, on emotional learning. The American journal of psychiatry. 2011; 168:163–172. [PubMed: 21123312]

Autio H, Matlik K, Rantamaki T, Lindemann L, Hoener MC, Chao M, Arumae U, Castren E. Acetylcholinesterase inhibitors rapidly activate Trk neurotrophin receptors in the mouse hippocampus. Neuropharmacology. 2011; 61:1291–1296. [PubMed: 21820453]

Begenisic T, Baroncelli L, Sansevero G, Milanese M, Bonifacino T, Bonanno G, Cioni G, Maffei L, Sale A. Fluoxetine in adulthood normalizes GABA release and rescues hippocampal synaptic plasticity and spatial memory in a mouse model of Down syndrome. Neurobiology of disease. 2014; 63:12–19. [PubMed: 24269730]

Begenisic T, Spolidoro M, Braschi C, Baroncelli L, Milanese M, Pietra G, Fabbri ME, Bonanno G, Cioni G, Maffei L, Sale A. Environmental enrichment decreases GABAergic inhibition and improves cognitive abilities, synaptic plasticity, and visual functions in a mouse model of Down syndrome. Front Cell Neurosci. 2011; 5:29. [PubMed: 22207837]

Belichenko NP, Belichenko PV, Kleschevnikov AM, Salehi A, Reeves RH, Mobley WC. The "Down syndrome critical region" is sufficient in the mouse model to confer behavioral, neurophysiological,

and synaptic phenotypes characteristic of Down syndrome. J Neurosci. 2009a; 29:5938–5948. [PubMed: 19420260]

Belichenko PV, Kleschevnikov AM, Masliah E, Wu C, Takimoto-Kimura R, Salehi A, Mobley WC. Excitatory-inhibitory relationship in the fascia dentata in the Ts65Dn mouse model of Down syndrome. J Comp Neurol. 2009b; 512:453–466. [PubMed: 19034952]

Belichenko PV, Masliah E, Kleschevnikov AM, Villar AJ, Epstein CJ, Salehi A, Mobley WC. Synaptic structural abnormalities in the Ts65Dn mouse model of Down Syndrome. The Journal of comparative neurology. 2004; 480:281–298. [PubMed: 15515178]

Burger PC, Vogel FS. The development of the pathologic changes of Alzheimer's disease and senile dementia in patients with Down's syndrome. Am J Pathol. 1973; 73:457–476. [PubMed: 4271339]

Cataldo AM, Barnett JL, Pieroni C, Nixon RA. Increased neuronal endocytosis and protease delivery to early endosomes in sporadic Alzheimer's disease: neuropathologic evidence for a mechanism of increased beta-amyloidogenesis. J Neurosci. 1997; 17:6142–6151. [PubMed: 9236226]

Cataldo AM, Mathews PM, Boiteau AB, Hassinger LC, Peterhoff CM, Jiang Y, Mullaney K, Neve RL, Gruenberg J, Nixon RA. Down syndrome fibroblast model of Alzheimer-related endosome pathology: accelerated endocytosis promotes late endocytic defects. The American journal of pathology. 2008; 173:370–384. [PubMed: 18535180]

Cataldo AM, Petanceska S, Peterhoff CM, Terio NB, Epstein CJ, Villar A, Carlson EJ, Staufenbiel M, Nixon RA. App gene dosage modulates endosomal abnormalities of Alzheimer.ıs disease in a segmental trisomy 16 mouse model of down syndrome. J Neurosci. 2003; 23:6788–6792. [PubMed: 12890772]

Cataldo AM, Peterhoff CM, Troncoso JC, Gomez-Isla T, Hyman BT, Nixon RA. Endocytic pathway abnormalities precede amyloid beta deposition in sporadic Alzheimer's disease and Down syndrome: differential effects of APOE genotype and presenilin mutations. The American journal of pathology. 2000; 157:277–286. [PubMed: 10880397]

Chakrabarti L, Galdzicki Z, Haydar TF. Defects in embryonic neurogenesis and initial synapse formation in the forebrain of the Ts65Dn mouse model of Down syndrome. J Neurosci. 2007; 27:11483–11495. [PubMed: 17959791]

Chapman RS, Hesketh LJ. Behavioral phenotype of individuals with Down syndrome. Ment Retard Dev Disabil Res Rev. 2000; 6:84–95. [PubMed: 10899801]

Chen AI, Nguyen CN, Copenhagen DR, Badurek S, Minichiello L, Ranscht B, Reichardt LF. TrkB (tropomyosin-related kinase B) controls the assembly and maintenance of GABAergic synapses in the cerebellar cortex. J Neurosci. 2011a; 31:2769–2780. [PubMed: 21414899]

Chen JL, Lin WC, Cha JW, So PT, Kubota Y, Nedivi E. Structural basis for the role of inhibition in facilitating adult brain plasticity. Nature neuroscience. 2011b; 14:587–594. [PubMed: 21478885]

Chen LY, Rex CS, Sanaiha Y, Lynch G, Gall CM. Learning induces neurotrophin signaling at hippocampal synapses. Proc Natl Acad Sci U S A. 2010; 107:7030–7035. [PubMed: 20356829]

Cooper JD, Salehi A, Delcroix JD, Howe CL, Belichenko PV, Chua-Couzens J, Kilbridge JF, Carlson EJ, Epstein CJ, Mobley WC. Failed retrograde transport of NGF in a mouse model of Down's syndrome: reversal of cholinergic neurodegenerative phenotypes following NGF infusion. Proceedings of the National Academy of Sciences of the United States of America. 2001a; 98:10439–10444. [PubMed: 11504920]

Cooper JD, Salehi A, Delcroix JD, Howe CL, Belichenko PV, Chua-Couzens J, Kilbridge JF, Carlson EJ, Epstein CJ, Mobley WC. Failed retrograde transport of NGF in a mouse model of Down's syndrome: reversal of cholinergic neurodegenerative phenotypes following NGF infusion. Proc Natl Acad Sci U S A. 2001b; 98:10439–10444. [PubMed: 11504920]

Deinhardt K, Salinas S, Verastegui C, Watson R, Worth D, Hanrahan S, Bucci C, Schiavo G. Rab5 and Rab7 control endocytic sorting along the axonal retrograde transport pathway. Neuron. 2006; 52:293–305. [PubMed: 17046692]

Dorsey SG, Bambrick LL, Balice-Gordon RJ, Krueger BK. Failure of brain-derived neurotrophic factor-dependent neuron survival in mouse trisomy 16. J Neurosci. 2002; 22:2571–2578. [PubMed: 11923422]

Ellis WG, McCulloch JR, Corley CL. Presenile dementia in Down's syndrome. Ultrastructural identity with Alzheimer's disease. Neurology. 1974; 24:101–106. [PubMed: 4272520]

Feng G, Mellor RH, Bernstein M, Keller-Peck C, Nguyen QT, Wallace M, Nerbonne JM, Lichtman JW, Sanes JR. Imaging neuronal subsets in transgenic mice expressing multiple spectral variants of GFP. Neuron. 2000; 28:41–51. [PubMed: 11086982]

Fernandez F, Morishita W, Zuniga E, Nguyen J, Blank M, Malenka RC, Garner CC. Pharmacotherapy for cognitive impairment in a mouse model of Down syndrome. Nature neuroscience. 2007; 10:411–413. [PubMed: 17322876]

Ferrer I, Gullotta F. Down's syndrome and Alzheimer's disease: dendritic spine counts in the hippocampus. Acta Neuropathol. 1990; 79:680–685. [PubMed: 2141748]

Fletcher JM, Morton CJ, Zwar RA, Murray SS, O'Leary PD, Hughes RA. Design of a conformationally defined and proteolytically stable circular mimetic of brain-derived neurotrophic factor. J Biol Chem. 2008; 283:33375–33383. [PubMed: 18809686]

Ginsberg SD, Alldred MJ, Counts SE, Cataldo AM, Neve RL, Jiang Y, Wuu J, Chao MV, Mufson EJ, Nixon RA, Che S. Microarray analysis of hippocampal CA1 neurons implicates early endosomal dysfunction during Alzheimer's disease progression. Biol Psychiatry. 2010; 68:885–893. [PubMed: 20655510]

Gorski JA, Zeiler SR, Tamowski S, Jones KR. Brain-derived neurotrophic factor is required for the maintenance of cortical dendrites. J Neurosci. 2003; 23:6856–6865. [PubMed: 12890780]

Grimes ML, Zhou J, Beattie EC, Yuen EC, Hall DE, Valletta JS, Topp KS, LaVail JH, Bunnett NW, Mobley WC. Endocytosis of activated TrkA: evidence that nerve growth factor induces formation of signaling endosomes. J Neurosci. 1996; 16:7950–7964. [PubMed: 8987823]

Hohmann CF, Wilson L, Coyle JT. Efferent and afferent connections of mouse sensory-motor cortex following cholinergic deafferentation at birth. Cerebral cortex. 1991; 1:158–172. [PubMed: 1726604]

Huang YZ, McNamara JO. Neuroprotective effects of reactive oxygen species mediated by BDNF-independent activation of TrkB. J Neurosci. 2012; 32:15521–15532. [PubMed: 23115189]

Itami C, Kimura F, Kohno T, Matsuoka M, Ichikawa M, Tsumoto T, Nakamura S. Brain-derived neurotrophic factor-dependent unmasking of "silent" synapses in the developing mouse barrel cortex. Proc Natl Acad Sci U S A. 2003; 100:13069–13074. [PubMed: 14557544]

Itami C, Kimura F, Nakamura S. Brain-derived neurotrophic factor regulates the maturation of layer 4 fast-spiking cells after the second postnatal week in the developing barrel cortex. J Neurosci. 2007; 27:2241–2252. [PubMed: 17329421]

Jiao Y, Zhang Z, Zhang C, Wang X, Sakata K, Lu B, Sun QQ. A key mechanism underlying sensory experience-dependent maturation of neocortical GABAergic circuits in vivo. Proc Natl Acad Sci U S A. 2011; 108:12131–12136. [PubMed: 21730187]

Kang H, Schuman EM. Long-lasting neurotrophin-induced enhancement of synaptic transmission in the adult hippocampus. Science. 1995; 267:1658–1662. [PubMed: 7886457]

Klein R, Conway D, Parada LF, Barbacid M. The trkB tyrosine protein kinase gene codes for a second neurogenic receptor that lacks the catalytic kinase domain. Cell. 1990; 61:647–656. [PubMed: 2160854]

Kleschevnikov AM, Belichenko PV, Gall J, George L, Nosheny R, Maloney MT, Salehi A, Mobley WC. Increased efficiency of the GABAA and GABAB receptor-mediated neurotransmission in the Ts65Dn mouse model of Down syndrome. Neurobiology of disease. 2012a; 45:683–691. [PubMed: 22062771]

Kleschevnikov AM, Belichenko PV, Gall J, George L, Nosheny R, Maloney MT, Salehi A, Mobley WC. Increased efficiency of the GABAA and GABAB receptor-mediated neurotransmission in the Ts65Dn mouse model of Down syndrome. Neurobiol Dis. 2012b; 45:683–691. [PubMed: 22062771]

Kleschevnikov AM, Belichenko PV, Villar AJ, Epstein CJ, Malenka RC, Mobley WC. Hippocampal long-term potentiation suppressed by increased inhibition in the Ts65Dn mouse, a genetic model of Down syndrome. J Neurosci. 2004; 24:8153–8160. [PubMed: 15371516]

Knusel B, Rabin S, Widmer HR, Hefti F, Kaplan DR. Neurotrophin-induced trk receptor phosphorylation and cholinergic neuron response in primary cultures of embryonic rat brain neurons. Neuroreport. 1992; 3:885–888. [PubMed: 1421094]

Kurt MA, Kafa MI, Dierssen M, Davies DC. Deficits of neuronal density in CA1 and synaptic density in the dentate gyrus, CA3 and CA1, in a mouse model of Down syndrome. Brain Res. 2004; 1022:101–109. [PubMed: 15353219]

Lai F, Williams RS. A prospective study of Alzheimer disease in Down syndrome. Arch Neurol. 1989; 46:849–853. [PubMed: 2527024]

Lush ME, Ma L, Parada LF. TrkB signaling regulates the developmental maturation of the somatosensory cortex. Int J Dev Neurosci. 2005; 23:523–536. [PubMed: 16009525]

Micheva KD, Busse B, Weiler NC, O'Rourke N, Smith SJ. Single-synapse analysis of a diverse synapse population: proteomic imaging methods and markers. Neuron. 2010a; 68:639–653. [PubMed: 21092855]

Micheva KD, O'Rourke N, Busse B, Smith SJ. Array tomography: high-resolution three-dimensional immunofluorescence. Cold Spring Harb Protoc. 2010b 2010 pdb top89.

Micheva KD, O'Rourke N, Busse B, Smith SJ. Array tomography: production of arrays. Cold Spring Harb Protoc. 2010c 2010 pdb prot5524.

Micheva KD, Smith SJ. Array tomography: a new tool for imaging the molecular architecture and ultrastructure of neural circuits. Neuron. 2007; 55:25–36. [PubMed: 17610815]

Mitra A, Blank M, Madison DV. Developmentally altered inhibition in Ts65Dn, a mouse model of Down syndrome. Brain research. 2012; 1440:1–8. [PubMed: 22284618]

Nikolaev A, McLaughlin T, O'Leary DD, Tessier-Lavigne M. APP binds DR6 to trigger axon pruning and neuron death via distinct caspases. Nature. 2009; 457:981–989. [PubMed: 19225519]

Oda K, Matsuoka Y, Funahashi A, Kitano H. A comprehensive pathway map of epidermal growth factor receptor signaling. Mol Syst Biol. 2005; 1 2005 0010.

Patz S, Wirth MJ, Gorba T, Klostermann O, Wahle P. Neuronal activity and neurotrophic factors regulate GAD-65/67 mRNA and protein expression in organotypic cultures of rat visual cortex. Eur J Neurosci. 2003; 18:1–12. [PubMed: 12859332]

Price DL, Whitehouse PJ, Struble RG, Coyle JT, Clark AW, Delong MR, Cork LC, Hedreen JC. Alzheimer's disease and Down's syndrome. Ann N Y Acad Sci. 1982; 396:145–164. [PubMed: 6217772]

Reeves RH, Irving NG, Moran TH, Wohn A, Kitt C, Sisodia SS, Schmidt C, Bronson RT, Davisson MT. A mouse model for Down syndrome exhibits learning and behaviour deficits. Nature genetics. 1995; 11:177–184. [PubMed: 7550346]

Rico B, Xu B, Reichardt LF. TrkB receptor signaling is required for establishment of GABAergic synapses in the cerebellum. Nature neuroscience. 2002; 5:225–233. [PubMed: 11836532]

Rissman RA, Mobley WC. Implications for treatment: GABAA receptors in aging, Down syndrome and Alzheimer's disease. J Neurochem. 2011; 117:613–622. [PubMed: 21388375]

Salehi A, Delcroix JD, Belichenko PV, Zhan K, Wu C, Valletta JS, Takimoto-Kimura R, Kleschevnikov AM, Sambamurti K, Chung PP, Xia W, Villar A, Campbell WA, Kulnane LS, Nixon RA, Lamb BT, Epstein CJ, Stokin GB, Goldstein LS, Mobley WC. Increased App expression in a mouse model of Down's syndrome disrupts NGF transport and causes cholinergic neuron degeneration. Neuron. 2006; 51:29–42. [PubMed: 16815330]

Sanchez-Huertas C, Rico B. CREB-Dependent Regulation of GAD65 Transcription by BDNF/TrkB in Cortical Interneurons. Cereb Cortex. 2011; 21:777–788. [PubMed: 20739478]

Seil FJ, Drake-Baumann R. TrkB receptor ligands promote activity-dependent inhibitory synaptogenesis. J Neurosci. 2000; 20:5367–5373. [PubMed: 10884321]

Siarey RJ, Stoll J, Rapoport SI, Galdzicki Z. Altered long-term potentiation in the young and old Ts65Dn mouse, a model for Down Syndrome. Neuropharmacology. 1997; 36:1549–1554. [PubMed: 9517425]

Thomson AM, Lamy C. Functional maps of neocortical local circuitry. Front Neurosci. 2007; 1:19–42. [PubMed: 18982117]

Troca-Marin JA, Alves-Sampaio A, Montesinos ML. An increase in basal BDNF provokes hyperactivation of the Akt-mammalian target of rapamycin pathway and deregulation of local dendritic translation in a mouse model of Down's syndrome. J Neurosci. 2011; 31:9445–9455. [PubMed: 21715609]

Valdez G, Akmentin W, Philippidou P, Kuruvilla R, Ginty DD, Halegoua S. Pincher-mediated macroendocytosis underlies retrograde signaling by neurotrophin receptors. J Neurosci. 2005; 25:5236–5247. [PubMed: 15917464]

van Steensel B, van Binnendijk EP, Hornsby CD, van der Voort HT, Krozowski ZS, de Kloet ER, van Driel R. Partial colocalization of glucocorticoid and mineralocorticoid receptors in discrete compartments in nuclei of rat hippocampus neurons. J Cell Sci. 1996; 109(Pt 4):787–792. [PubMed: 8718670]

Weitzdoerfer R, Dierssen M, Fountoulakis M, Lubec G. Fetal life in Down syndrome starts with normal neuronal density but impaired dendritic spines and synaptosomal structure. J Neural Transm Suppl. 2001:59–70. [PubMed: 11771761]

Yamada MK, Nakanishi K, Ohba S, Nakamura T, Ikegaya Y, Nishiyama N, Matsuki N. Brain-derived neurotrophic factor promotes the maturation of GABAergic mechanisms in cultured hippocampal neurons. J Neurosci. 2002; 22:7580–7585. [PubMed: 12196581]

Yin J, Yuan Q. Structural homeostasis in the nervous system: a balancing act for wiring plasticity and stability. Frontiers in cellular neuroscience. 2014; 8:439. [PubMed: 25653587]

Yoshii A, Constantine-Paton M. BDNF induces transport of PSD-95 to dendrites through PI3K–AKT signaling after NMDA receptor activation. Nature neuroscience. 2007; 10:702–711. [PubMed: 17515902]

Zirrgiebel U, Ohga Y, Carter B, Berninger B, Inagaki N, Thoenen H, Lindholm D. Characterization of TrkB receptor-mediated signaling pathways in rat cerebellar granule neurons: involvement of protein kinase C in neuronal survival. J Neurochem. 1995; 65:2241–2250. [PubMed: 7595513]

Highlights

- TrkB signaling, including MAPK and PI3K, were increased in Ts65Dn cortex.
- Increased pTrkB signaling was present in synapses and signaling endosomes.
- Array tomography showed an increase in the ratio of GABAergic to glutamatergic synapses.
- TrkB signaling was dramatically increased in GABAergic synapses.
- Increased TrkB signaling in cortical circuits may contribute to cognitive deficits.

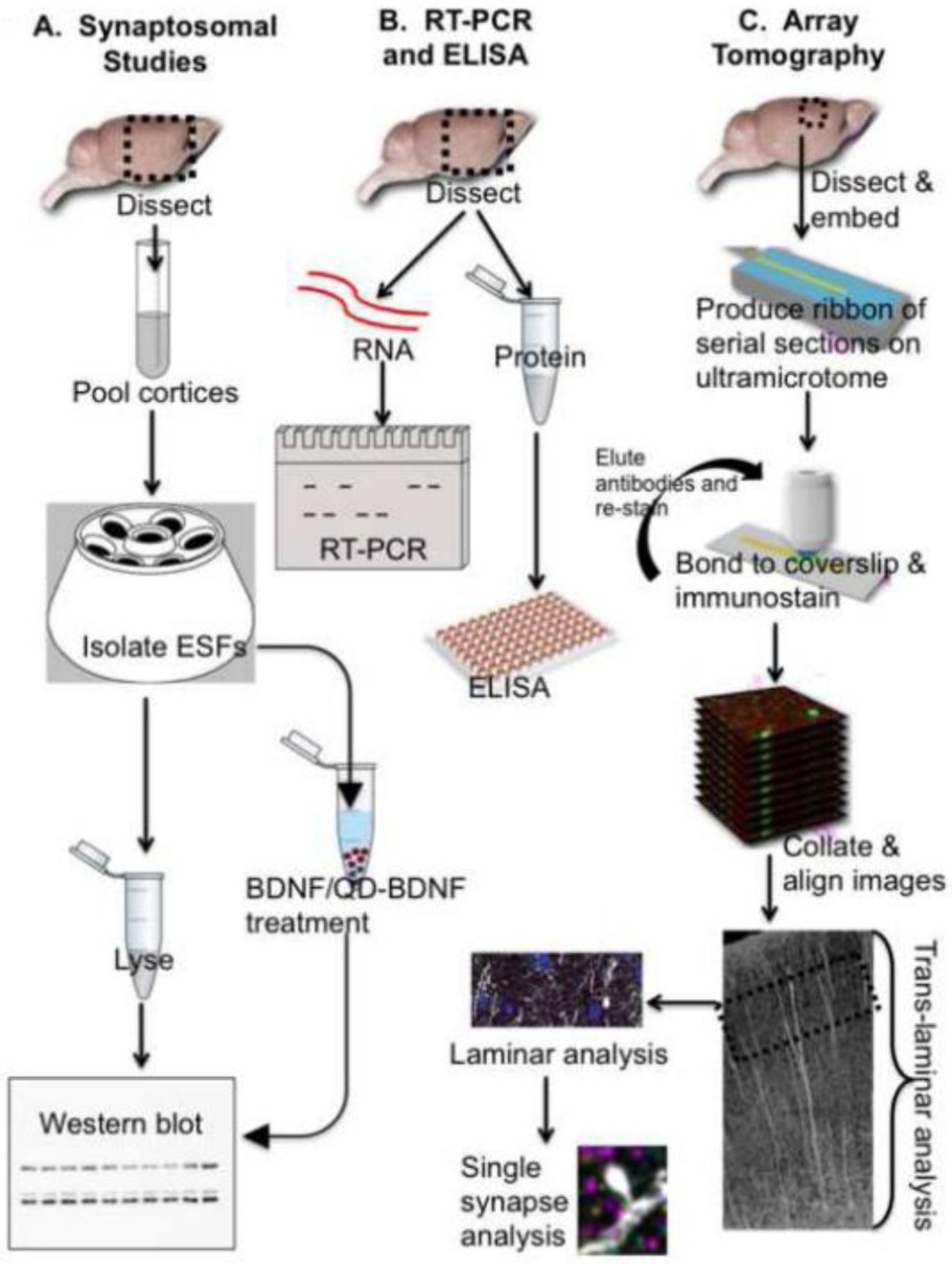

Figure 1. Flow diagram of the overall experimental approach

Three main experimental approaches give unique but complementary information. Synaptosomal studies (**A**) isolate an enriched synaptosomal fragment (ESF), allowing us to amplify synaptic signals, but do not permit us to distinguish synaptic subtypes. RT-PCR and ELISA studies (**B**) provide information about global differences in mRNA and protein in somatosensory cortex. Array tomography (**C**) enables us to determine proteomic changes at the single synapse level of resolution, to interrogate the status of specific synaptic subtypes, and to identify cortical layer-specific changes.

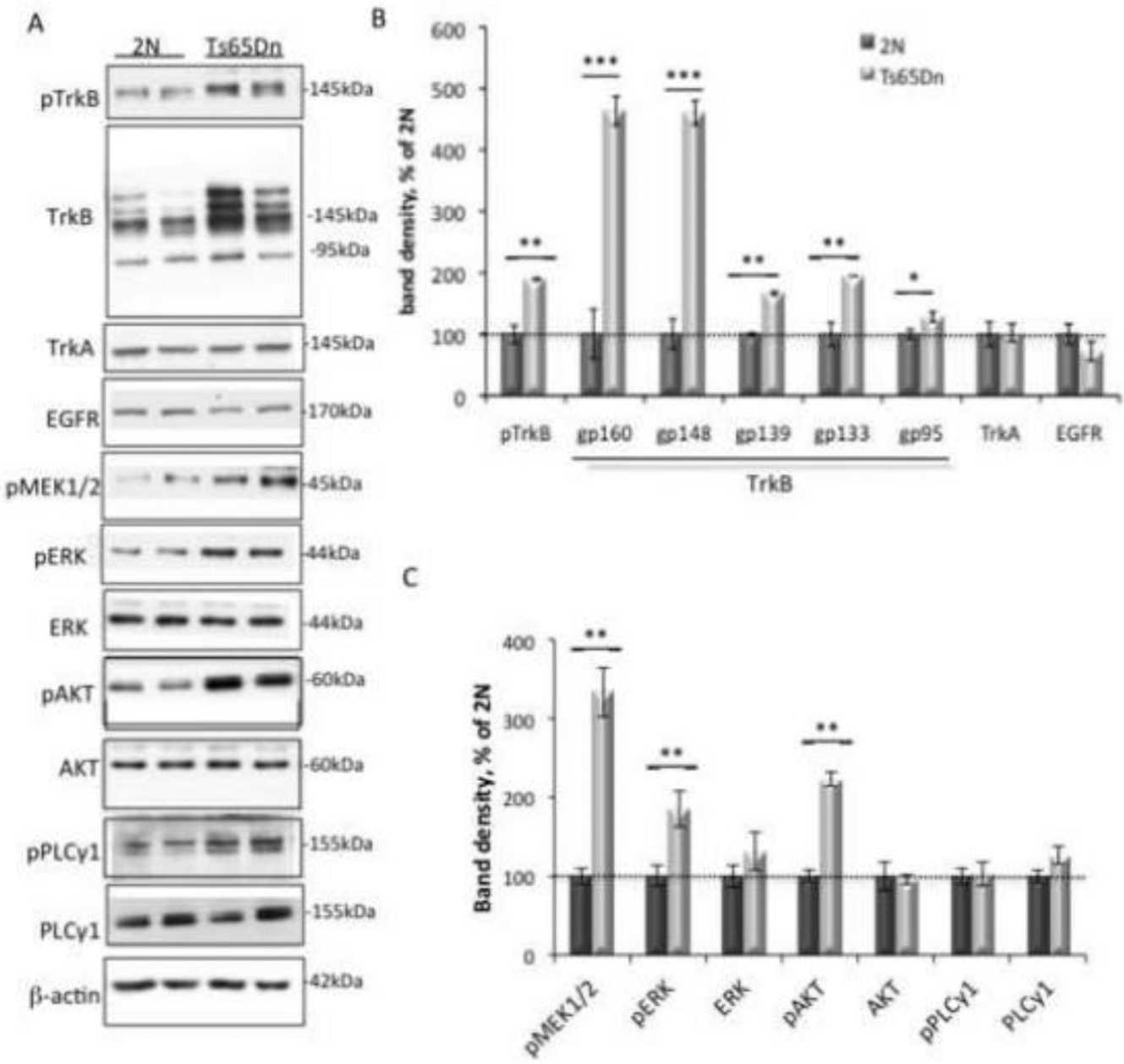

Figure 2. Excessive TrkB signaling in Ts65Dn synaptosomes

(A) Representative WB of cortical synaptosomal lysates immunoblotted with antibodies against the tyrosine-phosphorylated receptors TrkB, TrkA, EGFR, MAPK, PI3K, PLCγ-related signaling proteins, and β-actin as a control for total protein levels. **(B and C)** Quantitative analysis of WB data showing a significant increase in total TrkB, pTrkB, pMEK1/2, pERK, and pAKT in Ts65Dn synaptosomes. Data are expressed as mean ± SEM percent of 2N values, n = 6 per genotype. *p<0.05, **p<0.005, ***p<0.0005, versus 2N.

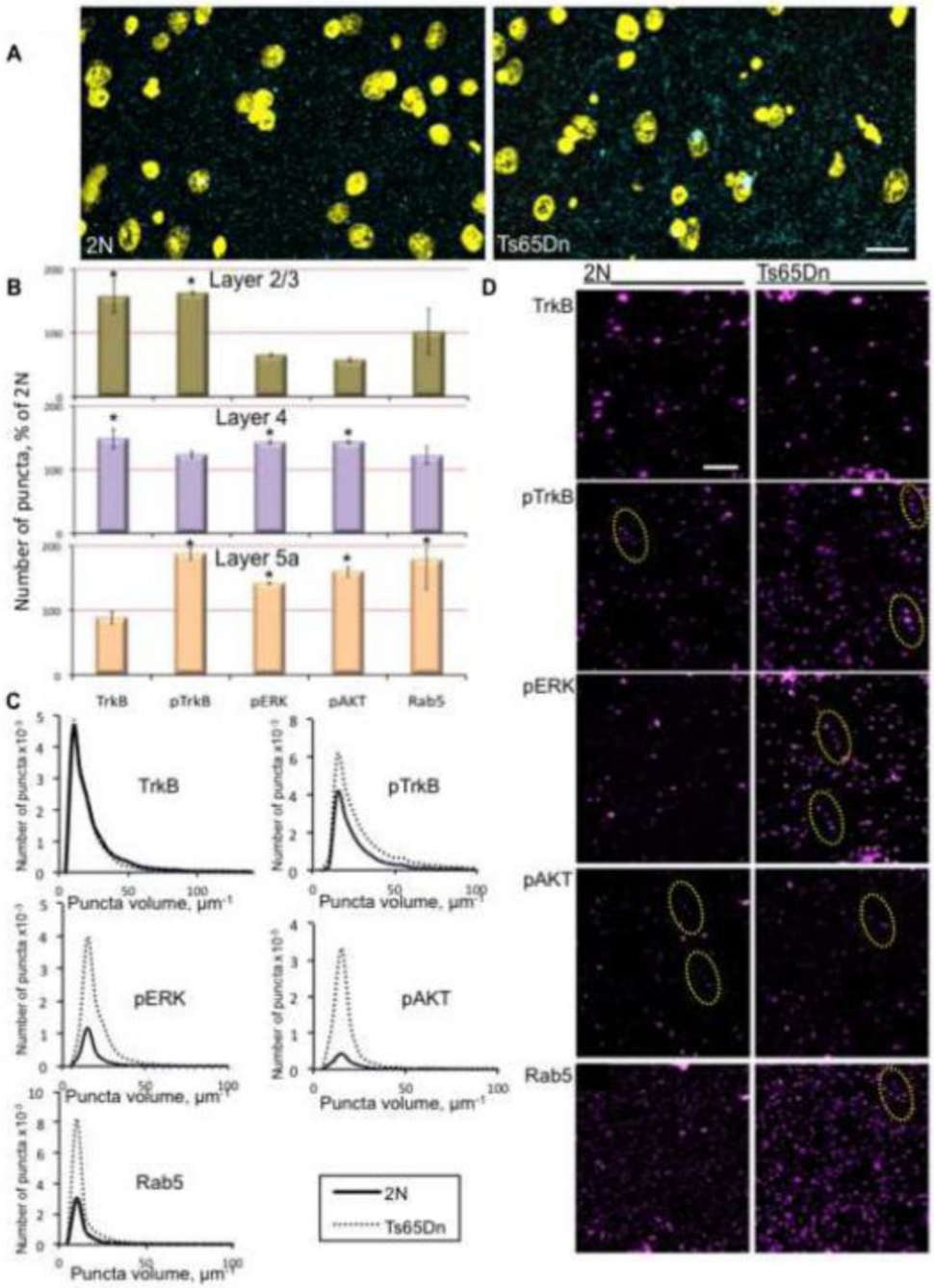

Figure 3. Array tomographic analysis of pTrkB signaling in 2N and Ts65Dn somatosensory cortex

(A) Representative cortical volume renderings from a 2N and Ts65Dn mouse demonstrating the ability of AT to segment individual pTrkB puncta (cyan) in a large volume. DAPI = yellow; bar = 100 µm. **(B)** Quantification of the number of puncta in cortex layers 2/3, 4, and 5a of Ts65Dn and 2N mice. Data are expressed as mean ± SEM percent of 2N values. *p<0.05, versus 2N. **(C)** Volume distribution of puncta positive for various markers in layer 5a cortex of 2N and Ts65Dn mice. n=3 per genotype. **(D)** Representative cortical volume

reconstructions from a 2N and Ts65Dn mouse showing TrkB, pTrkB , pERK, pAKT, and Rab5 positive puncta in layer 5a cortex. For pTrkB, pERK, and pAKT, the staining pattern included puncta arranged in an apparent “beads on a string” pattern (dashed yellow ovals), consistent with proteins present in processes. Bar = 2 μm.

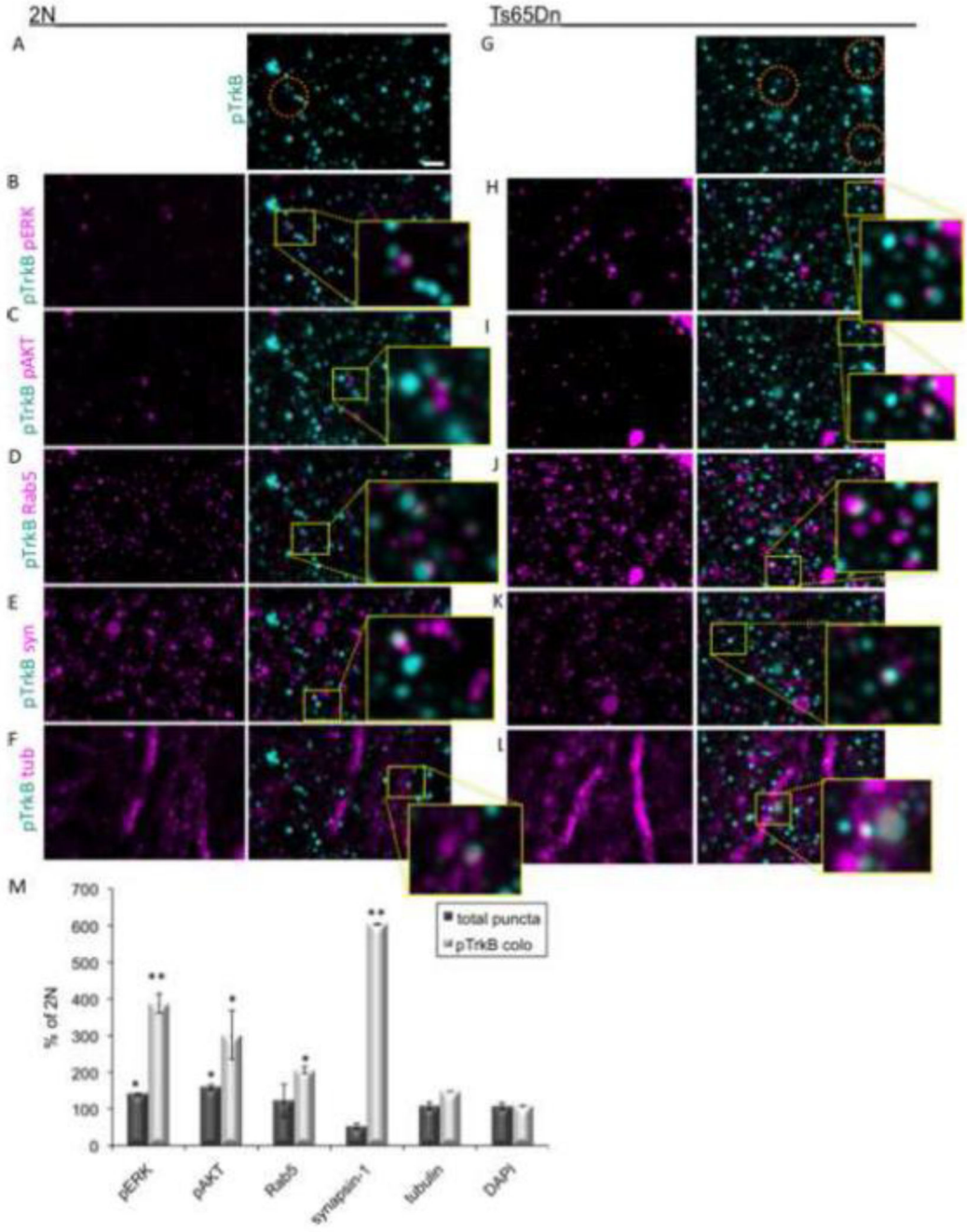

Figure 4. Sub-cellular localization of pTrkB in layer 4 of the Ts65Dn somatosensory cortex

(**A–L)** Representative cortical volume reconstructions from a 2N (**A–F**) and Ts65Dn (**G–L**) mouse showing colocalization of TrkB (cyan, **A** and **G**) with various markers in magenta: pERK (**B and H**), pAKT (**C and I**), Rab5 **(D and J**), synapsin-1 (syn, **E and K**), and α-tubulin (tub, **F** and **L**). Area inside the yellow rectangles are shown at higher magnification to better visualize colocalization of pTrkB and the various markers. Orange ovals in A and G indicate possible signaling endosomes, which are positive for pTrkB, Rab5, and either pERK or pAKT. Bar = 2 μm. **(M)** Quantification of the total puncta number (dark bars) and

the normalized colocalization with pTrkB (light bars) for the indicated markers. Data are expressed as mean ± SEM percent of 2N values. *p<0.05, **p<0.005 versus 2N. n = 3 per genotype.

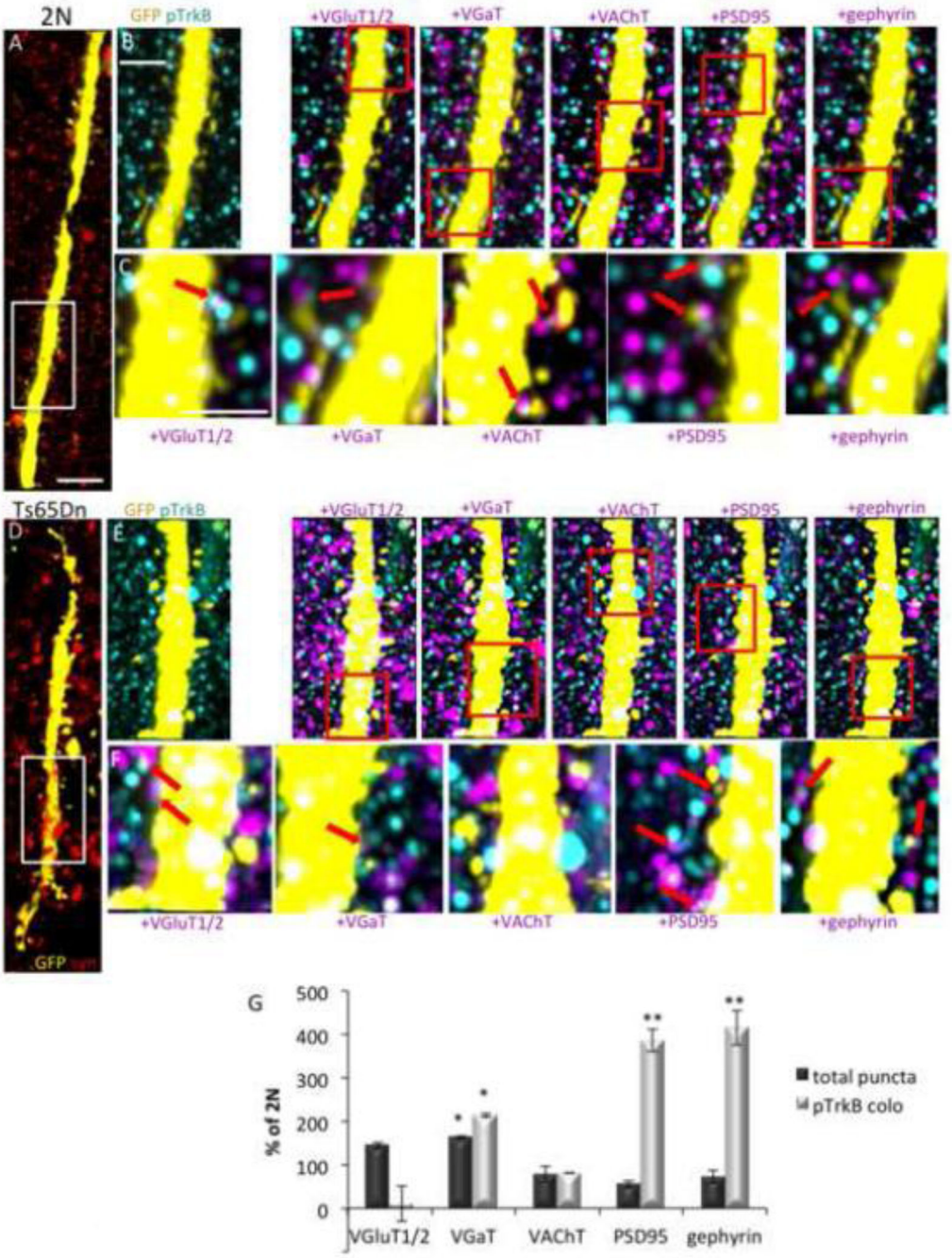

Figure 5. Analysis of pTrkB colocalization with synaptic markers

(A–F) Representative volume renderings of cortical arrays from a 2N **(A–C)** and Ts65Dn **(D–F)** mouse. **A and D** shows all synapses (synapsin-1, red) surrounding a GFP positive apical dendrite (yellow). Bar = 4 μm. **B and E** are higher magnification renderings of the area indicated by the white rectangles in **A and D**, showing colocalization of pTrkB (cyan) with the synaptic markers VGluT1/2, VGaT, VAChT, PSD95, and gephyrin (magenta) on synaptic boutons of a GFP positive dendrite (yellow) of a layer 5 pyramidal cell. White spots on the dendrite indicate areas of overlap between GFP and a single antigen (pTrkB or

the indicated synaptic marker). Bar = 2 μm. C and F are higher magnifications of the area indicated by the red rectangles in B and E. Red arrows point to examples of pTrkB colocalized with the indicated synaptic marker on GFP+ dendrites. Bar = 1 μm. **(G)** Quantification of the total number of synaptic puncta (dark bars) and their normalized colocalization with pTrkB (light bars) in 2N and Ts65Dn mice. Data are expressed as mean ± SEM percent of 2N values. n = 3 per genotype; *p<0.05, **p<0.005 versus 2N.

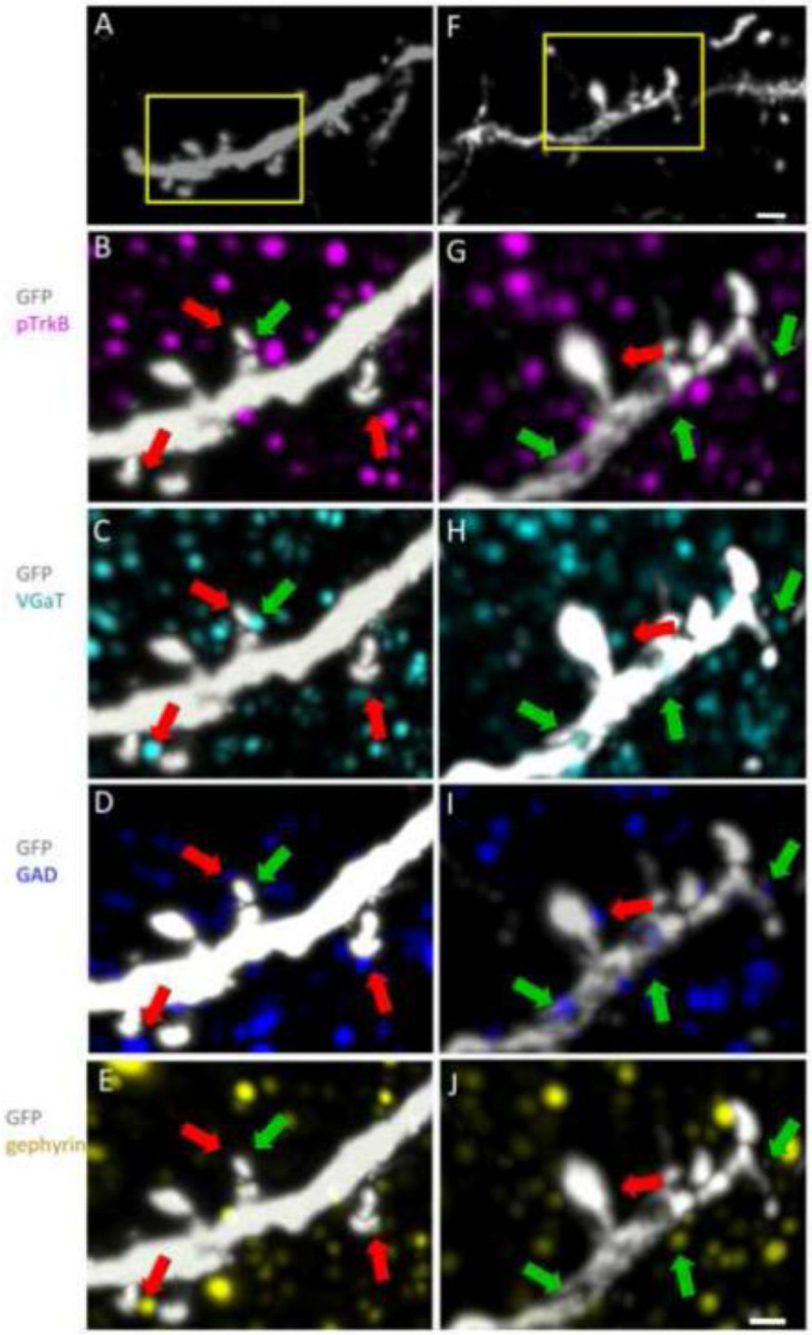

Figure 6. pTrkB in GABAergic synapses

(A and F) Volume renderings of a GFP (white) positive dendrite of a layer 5 pyramidal neuron from 2N **(A)** and Ts65Dn **(F)** cortex. Bar = 2 μm. **(B–J)** Higher magnification volume renderings of the areas indicated by the yellow rectangles in **A and F** show colocalization of pTrkB (magenta) with markers of GABAergic synapses in 2N **(B–E)** and Ts65Dn **(G–J)** cortical arrays. Green arrows point to examples of pTrkB positive GABAergic synapses. Red arrows point pTrkB negative GABAergic synapses. Bar = 1 μm.

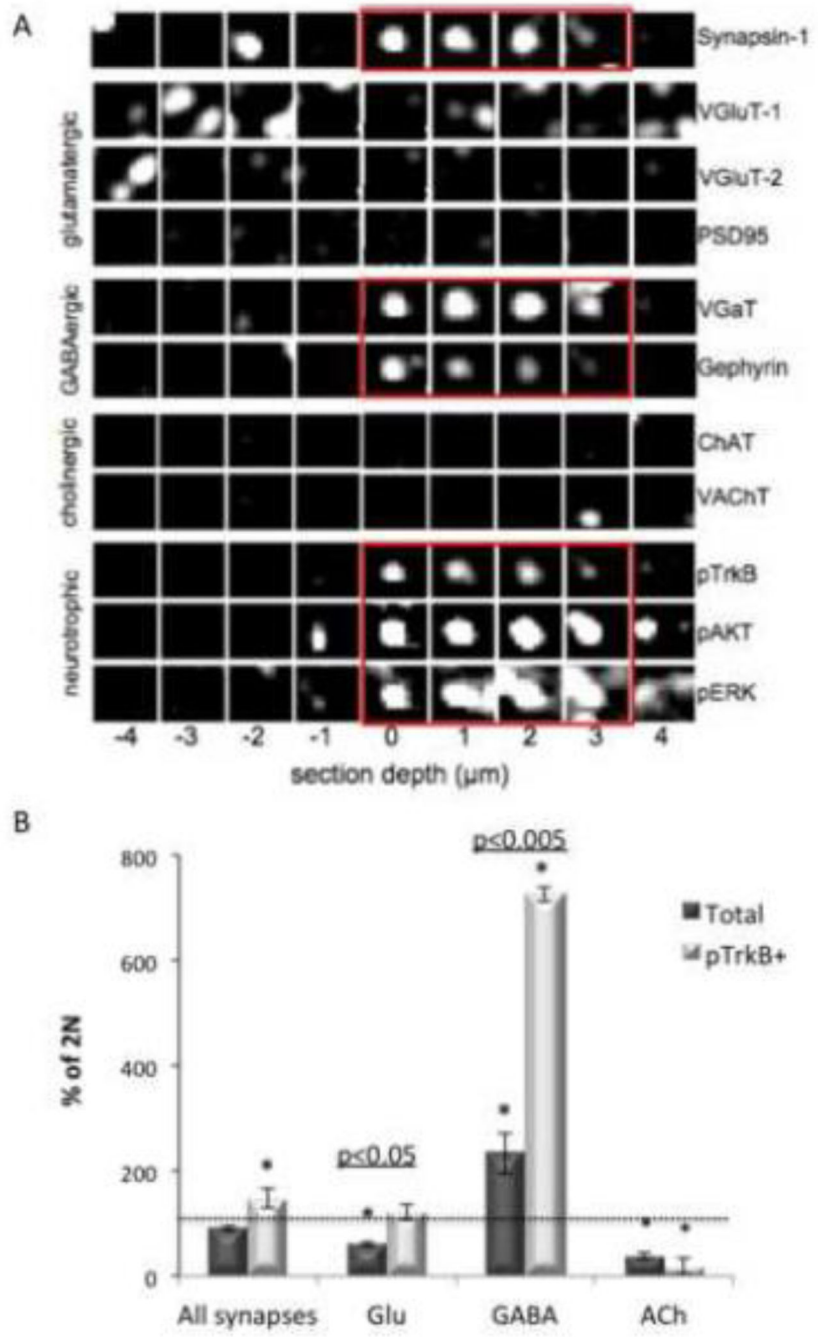

Figure 7. Classification of 2N and Ts65Dn cortical synapses

(**A**) A synaptogram generated from sequential staining and elution of the same ribbon of serial cortical sections from Ts65Dn somatosensory cortex layer 4. Columns represent one of nine serial sections, with section '0' located on the center of mass of a synapsin-1 punctum. Rows represent individual molecular markers as indicated. Synapsin-1 immunoreactivity overlaps with the channels highlighted in red. This GABAergic classified synapse is also positive for pTrkB and two related signaling molecules (red rectangles). (**B**) Quantification of classified synapse subtypes expressed as mean ± SEM percent of 2N

values. n = 3 per genotype. The total number of synapses classified per sample is 81,000-150,000. *p<0.05 versus 2N.

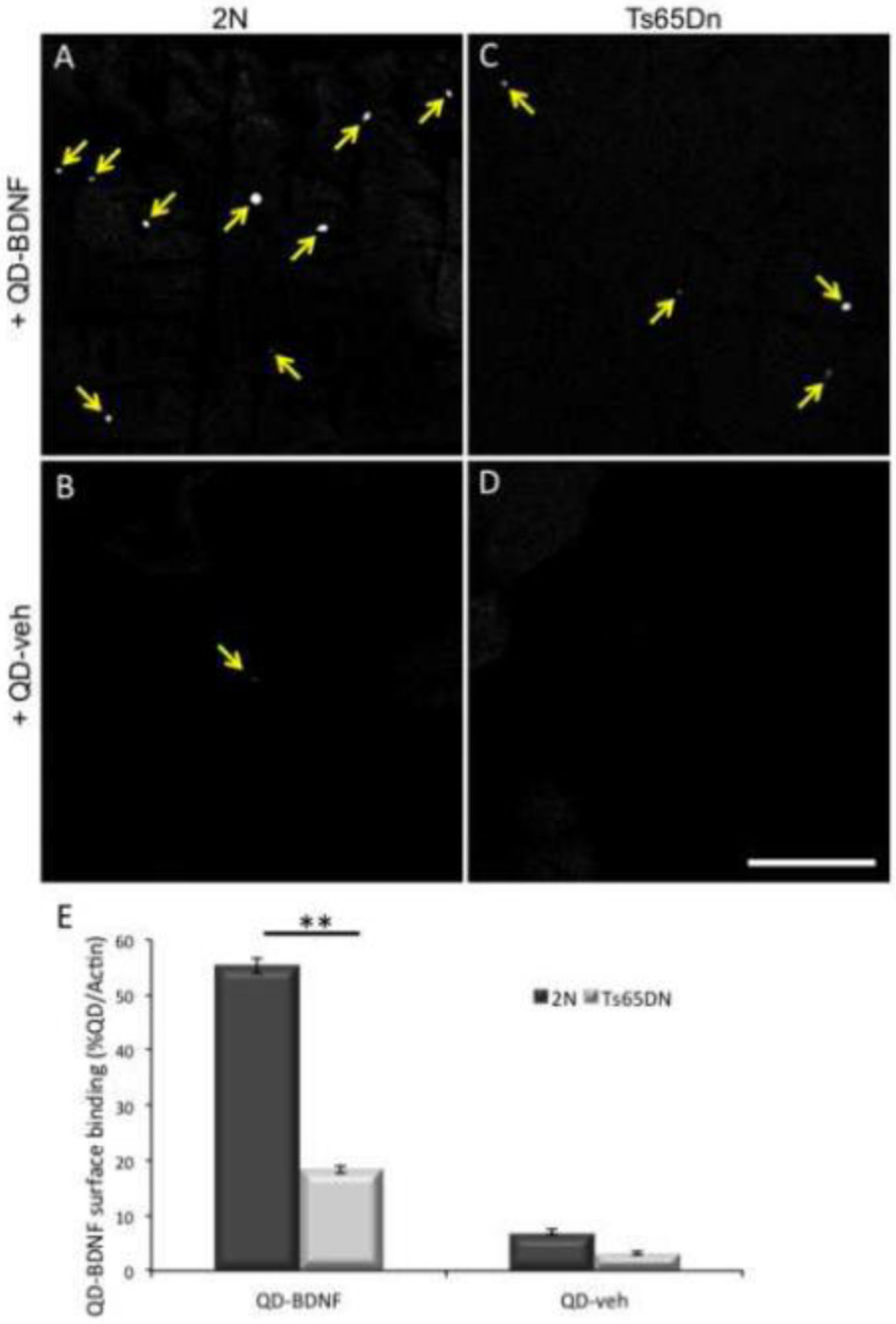

Figure 8. Decreased surface binding of BDNF in Ts65Dn synaptosomes

2N **(A and B)** and Ts65Dn **(C and D)** cortical synaptosomes were incubated with QD-BDNF (**A and C)** or QD alone (QD-veh, **B and D**). Yellow arrows indicate QD visualized on the surface of synaptosomes by confocal microscopy. Bar = 100μm. **(E)** The number of QD, normalized to the total number of actin positive synaptosomes, was quantified in each condition. n = 6 preps per genotype, ** $p<0.005$ versus 2N.

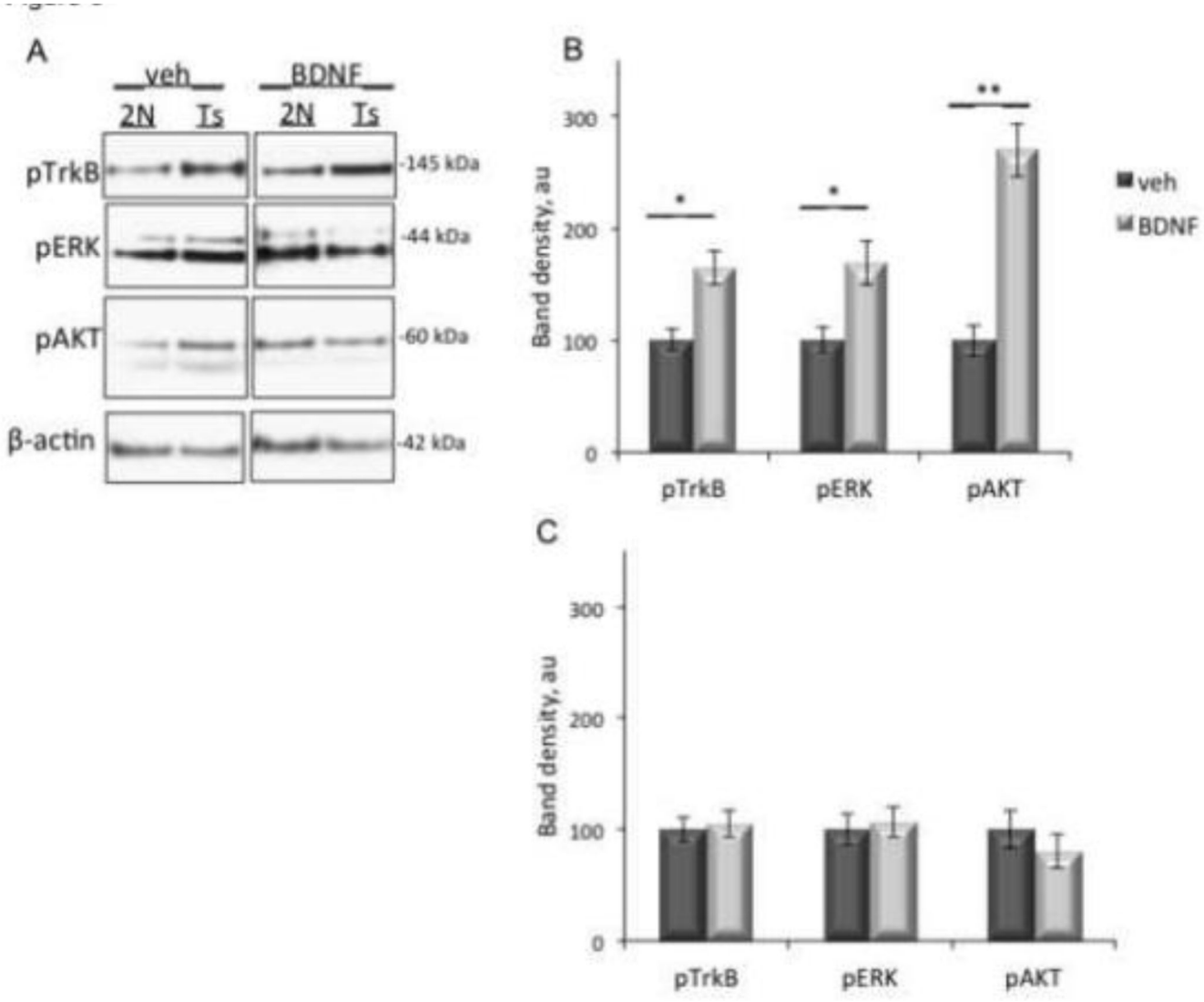

Figure 9. Blunted response of Ts65Dn synaptosomes to BDNF

(A) Cortical synaptosomes from 2N and Ts65Dn (Ts) mice were treated with BDNF or vehicle control (veh) prior to lysis and immunoblotting with antibodies against pTrkB, pERK, or pAKT. β-actin was used as an internal control for total protein levels. (**B and C)**. Quantification of band density in 2N (**B**) and Ts65Dn (**C**) synaptosomes, normalized to β-actin band density. Data are expressed as mean ± SEM. n = 6 per genotype. *p<0.05, **p<0.005, versus vehicle.

Table 1

pTrkB colocalization with individual sub-cellular and signaling markers.

	Percentage of pTrkB puncta colocalized	
Sub-cellular marker	**2N**	**Ts65Dn**
Synapsin-1	7.85 ± 0.26	24.33 ± 3.31*
Rab5	2.07 ± 0.02	4.25 ± 0.41*
pERK	1.19 ± 0.70	21.01 ± 5.54**
pAKT	2.19 ± 0.50	11.76 ± 7.86**
α-Tubulin	11.53 ± 0.60	26.00 ± 0.59*
DAPI	7.16 ± 2.27	11.73 ± 0.61

The percent of total pTrkB positive puncta that colocalize with each of the markers indicated in the left column for 2N and Ts65Dn cortical arrays. Data are expressed as mean ± SEM, n = 3 per genotype.

* $p<0.05$,

** $p<0.005$ versus 2N.

Table 2

pTrkB colocalization with individual synaptic markers

	Percentage of pTrkB puncta colocalized	
Synaptic marker	**2N**	**Ts65Dn**
Synapsin-1	7.85 ± 0.26	24.33 ± 3.31**
VGluT1	4.19 ± 0.39	4.08 ± 0.79
VGluT2	3.41 ± 0.16	0.92 ± 0.002*
VGaT	0.56 ± 0.10	3.36 ± 0.01*
VAChT	0.35 ± 0.01	0.87 ± 0.04
PSD95	1.58 ± 0.88	7.45 ± 0.67**
gephyrin	1.32 ± 0.09	12.09 ± 0.52 **

The percent of total pTrkB positive puncta that colocalize with each of the synaptic markers indicated in the left column is indicated for 2N and Ts65Dn cortical arrays. Data are expressed as mean ± SEM, n = 3 per genotype.

* $p<0.05$,

** $p<0.005$ versus 2N.